J. Fluid Mech. (1993), *vol.* 252, *pp.* 51–78

Singularity formation during Rayleigh–Taylor instability

By GREGORY BAKER,[1] RUSSEL E. CAFLISCH[2] AND MICHAEL SIEGEL[1]

[1] Mathematics Department, The Ohio State University, Columbus, OH 43210, USA

[2] Mathematics Department, UCLA, Los Angeles, CA 90024, USA

(Received 22 April 1992 and in revised form 12 January 1993)

During the motion of a fluid interface undergoing Rayleigh–Taylor instability, vorticity is generated on the interface baronclinically. This vorticity is then subject to Kelvin–Helmholtz instability. For the related problem of evolution of a nearly flat vortex sheet without density stratification (and with viscosity and surface tension neglected), Kelvin–Helmholtz instability has been shown to lead to development of curvature singularities in the sheet. In this paper, a simple approximate theory is developed for Rayleigh–Taylor instability as a generalization of Moore's approximation for vortex sheets. For the approximate theory, a family of exact solutions is found for which singularities develop on the fluid interface. The resulting predictions for the time and type of the singularity are directly verified by numerical computation of the full equations. These computations are performed using a point vortex method, and singularities for the numerical solution are detected using a form fit for the Fourier components at high wavenumber. Excellent agreement between the theoretical predictions and the numerical results is demonstrated for small to medium values of the Atwood number A, i.e. for A between 0 and approximately 0.9. For A near 1, however, the singularities actually slow down when close to the real axis. In particular, for $A = 1$, the numerical evidence suggests that the singularities do not reach the real axis in finite time.

1. Introduction

The classical manifestation of the Rayleigh–Taylor instability occurs when a heavy fluid lies above a lighter fluid in the presence of gravity. Sharp (1984) gives a general review of many experimental and theoretical studies. When the fluids are immiscible, a sharp interface exists between them which deforms into a pattern containing rising bubbles of lighter fluid and falling spikes of heavier fluid. A strong shearing flow develops on the sides of the spike as the lighter and heavier fluid pass by each other. This part of the interface is then susceptible to the Kelvin–Helmholtz instability. When the fluids are considered inviscid and incompressible, the shear flow region coincides with the interface, which may be represented as a vortex sheet whose strength changes by the baroclinic generation of vorticity. The growth rate for small disturbances subject to Kelvin–Helmholtz instability is much higher than for those subject to Rayleigh–Taylor instability. Consequently, the vortex sheet rolls up, so that the appearance of the spike changes to that associated with a falling plume of fluid in an ambient fluid.

Based on a vortex sheet representation, a set of evolution equations for the location of the interface has been derived by Baker, Meiron & Orszag (1982) (see also Moore

1982). Their numerical calculations ran into the traditional difficulties associated with the computation of the rollup of vortex sheets (Saffman & Baker 1979). By employing some regularization, Kerr (1986) and Tryggvason (1988) suppressed these difficulties and showed rolled-up interfaces at late times.

However, recent studies of the evolution of vortex sheets in homogeneous fluid have shed new light on their behaviour. For periodic disturbances from a flat sheet, the evidence is now quite strong that sheets with non-zero mean vorticity develop a curvature singularity in finite time. Asymptotic studies by Moore (1979, 1985) and by Caflisch, Orellana & Siegel (1990) show how singularities in the complex circulation plane move towards and reach the real axis in finite time, at which point a curvature singularity is observed physically. Numerical calculations by Baker (1990) confirm the formation and motion of these complex singularities for the aysmptotic equations. Numerical calculations for the full equations show direct evidence of the presence of singularities in the complex circulation plane, but in order to run the calculations up to the singularity time it is necessary to employ a spectral filter, first used by Krasny (1986*b*), and subsequently by Shelley (1992) to gain detailed information about the nature of the singularity. Subsequent numerical studies by Ely & Baker (1993), done in arbitrary precision to eliminate the effects of round-off errors, show that the spectral filter can be used reliably up to the time of singularity formation. However, no convergence in the shape of the vortex sheet occurs after the singularity time as the truncation error is reduced with higher resolution. A different numerical calculation by Meiron, Baker & Orszag (1982) that generated terms for the Taylor series expansion in time of the vortex sheet location also shows the formation of a curvature singularity in finite time. There is not much doubt that a curvature singularity occurs in finite time, but what is less certain is the precise nature of the sheet after the singularity time. Rigorous theory (Diperna & Majda 1987; Delort 1991) allows the existence of measured-valued solutions corresponding to vortex sheets for Euler's equations, but the theory does not address the question of smoothness of the sheets.

This paper will show that there is analogous singularity formation during Rayleigh–Taylor instability. Numerical evidence for singularities has already been supplied by Pugh (1989) for the Boussinesq limit. Our work will consider the full range of Atwood ratios, A. A related investigation of singularities for Boussinesq bubbles was performed by Pugh & Cowley (1993). These singularities in general are believed to immediately precede the rollup of the interface and are thus closely related to the rate of fluid mixing. In addition, these singularities and their dependence on the Atwood number appear to be the source of many of the numerical difficulties that have been experienced in numerical simulations of Rayleigh–Taylor instability. It is only by introducing some form of regularization that the singularities in the complex physical plane are prevented from reaching the real axis. Then numerical calculations have been able to proceed beyond the singularity time and show the formation of rolled-up vortex sheets. Krasny (1986*a*) employs a vortex 'blob' method for the Kelvin–Helmholtz instability, and Kerr (1986) adapts this approach for the Rayleigh–Taylor problem. Tryggvason (1988) uses a 'cloud-in-cell' technique, and Baker, Meiron & Orszag (1980) consider two interfaces with a fluid of intermediate density between them.

Our study of singularity formation during Rayleigh–Taylor instability is by two complementary approaches: an analytic theory that derives asymptotic equations and a set of numerical solutions for the full equations. Thus we are able to comment directly on the conditions for the reliability of the asymptotic approach, as well as address another interesting aspect of the behaviour in Rayleigh–Taylor instability, namely the behaviour when the lighter fluid is a gas whose motion is negligible. Under

these conditions, the Kelvin–Helmholtz instability is inoperable, and the expectation is that no singularity will occur.

First a simple approximate theory is developed for the Rayleigh–Taylor instability as a generalization of Moore's approximation for the Kelvin–Helmholtz instability. The approximate equations were first derived by Siegel (1989), and are obtained by considering the variable α which parameterizes the interface to be a complex-valued variable. The excellent agreement of this theory with the numerical results of Pugh (1989) in the Boussinesq case motivated the present study over the full range $0 < A \leqslant 1$. Siegel (1989) shows that the approximation is asymptotically valid for α in a strip containing the real axis when the deformation of the interface is small and singularities are far from the real axis. For the related Kelvin–Helmholtz instability, Cowley *et al.* (1993) have established that the approximation is also asymptotically valid in those regions of the complex plane where $\mathrm{Im}\{\alpha\} \gg 1$ and the interface has $O(1)$ deformation. In particular, these regions include the immediate neighbourhood of singularities.

In the present study, this theory is applied for large deformations and for singularities that are near to the real axis, which is beyond the range of its formal validity. Nevertheless explicit predictions for the time t_c and location of singularity formation and the type of singularities follow from a set of exact solutions for the approximate equations. These exact solutions consist of pure growing modes and can be found as travelling waves with complex speed. These predictions agree well with the results from numerical calculations of the full equations when the Atwood ratio is not too close to 1. When the Atwood ratio is close to 1, some aspects of the agreement break down. For unit Atwood ratio, the approximate equations predict the existence of a new type of singularity which is stronger than the singularities for $A \neq 1$ and which reaches the real axis in finite time. The numerical calculations indicate that this singularity does indeed exist in the complex plane and that it moves towards the real axis. However, the singularity slows down, suggesting that it may not reach the real axis in finite time. Since the time of this study, Tanveer (1992) has looked further at singularities for $A = 1$ and has given evidence that no real singularities do occur.

2. The equations of motion

We are concerned with the two-dimensional motion due to gravity of a fluid of density ρ_1 lying under a fluid of density ρ_2 with $\rho_1 \leqslant \rho_2$. For simplicity the fluids are assumed to be incompressible and inviscid, as well as irrotational (away from the interface), and the surface tension at the interface between the fluids is negligible. The interface between the two fluids may be described by a complex function $z(\alpha, t) = x(\alpha, t) + \mathrm{i}y(\alpha, t)$ in which α is a real parameter.

Define the velocities $\boldsymbol{u}_1$ and $\boldsymbol{u}_2$ as the limiting values at the interface of the fluid velocity in the lower and upper fluid. Conservation of mass requires that they have equal normal components, i.e.

$$\boldsymbol{n} \cdot \boldsymbol{u}_1 = \boldsymbol{n} \cdot \boldsymbol{u}_2. \tag{1}$$

In the absence of viscosity, however, the tangential components can be discontinuous. Thus the fluid interface is a slip line, or in other words a vortex sheet.

The vortex sheet strength along the interface, $\tilde{\gamma}$, is defined by

$$\tilde{\gamma} = (\boldsymbol{u}_1 - \boldsymbol{u}_2) \cdot \hat{\boldsymbol{s}}, \tag{2}$$

where $\hat{\boldsymbol{s}}$ is the unit tangent vector pointing to the right relative to the direction from

lower to upper fluid. It is also convenient to define the un-normalized vortex sheet strength γ by

$$\gamma = \tilde{\gamma} s_\alpha, \tag{3}$$

where $s_\alpha = |z_\alpha|$.

The parameter α is chosen to be 'Lagrangian', although, since the fluid velocity has a discontinuity along the interface, the choice of velocity $\boldsymbol{U}$ for boundary points is not unique. Following Baker *et al.* (1982), we choose $\boldsymbol{U}$ to be a weighted average of $\boldsymbol{u}_1$ and $\boldsymbol{u}_2$, i.e.

$$\boldsymbol{U} = \tfrac{1}{2}(1+\beta)\,\boldsymbol{u}_1 + \tfrac{1}{2}(1-\beta)\,\boldsymbol{u}_2. \tag{4}$$

Note that $\beta = -1$ corresponds to $\boldsymbol{U} = \boldsymbol{u}_2$, the velocity of the upper fluid, and $\beta = 0$ corresponds to $\boldsymbol{U} = \frac{1}{2}(\boldsymbol{u}_1 + \boldsymbol{u}_2)$, the average velocity. In our numerical calculations β is chosen as

$$\beta = -A, \tag{5}$$

where A is the Atwood number

$$A = \frac{\rho_2 - \rho_1}{\rho_2 + \rho_1}. \tag{6}$$

Note that the definition of A follows the convention used in studies of the Rayleigh–Taylor instability, while for internal waves with $\rho_1 > \rho_2$, A is usually given the opposite sign. The choice (5) is equivalent to defining

$$\boldsymbol{U} = \frac{\rho_1 \boldsymbol{U}_1 + \rho_2 \boldsymbol{U}_2}{\rho_1 + \rho_2}.$$

This choice of β also simplifies the analysis given in §4.

The motion of the interface and the baronclinic generation of vorticity on it are described by the following integro-differential equations, derived by Baker *et al.* (1982),

$$\bar{z}_t = \bar{q} + \frac{\beta\gamma}{2z_\alpha}, \tag{7}$$

$$\gamma_t = 2A\left[\mathrm{Re}\left\{\bar{q}_t z_\alpha - \frac{\beta\gamma q_\alpha}{2z_\alpha}\right\} + g\,\mathrm{Im}\{z_\alpha\}\right] + \frac{A+2\beta}{4}\frac{\partial}{\partial\alpha}\left(\frac{\gamma^2}{|z_\alpha|^2}\right), \tag{8}$$

in which Re and Im denote the real and imaginary parts, and where q is the complex velocity which is given by the Birkhoff–Rott principal value integral,

$$\bar{q}(\alpha, t) = \frac{1}{2\pi\mathrm{i}}\,\mathrm{PV}\int \frac{\gamma(\alpha', t)}{z(\alpha, t) - z(\alpha', t)}\,\mathrm{d}\alpha'. \tag{9}$$

Subscripts α and t refer to differentiation, and the bar over a variable indicates its complex conjugate. A similar set of equations was derived by Moore (1982).

A simple solution for (7) and (8) is

$$z(\alpha, t) = \alpha + \tfrac{1}{2}\beta\gamma_0 t, \quad \gamma(\alpha, t) = \gamma_0, \tag{10}$$

for any constant γ_0. The motion of the points corresponds to a translation along a flat interface with uniform vortex sheet strength γ_0, and so this motion would be an equilibrium solution in an Eulerian frame of reference. Usually in studies of the Rayleigh–Taylor instability, γ_0 is taken to be zero, but we leave it arbitrary for now. The linearized version of (7) and (8) about the flat interface (10) permits solutions of the form

$$z(\alpha, t) = \alpha + \tfrac{1}{2}\beta\gamma_0 t + A\,\mathrm{e}^{\mathrm{i}k\alpha \pm \sigma(k)t}, \quad \gamma(\alpha, t) = \gamma_0 + B\,\mathrm{e}^{\mathrm{i}k\alpha \pm \sigma(k)t}, \tag{11 a, b}$$

where
$$2\sigma(k) = ik(A+\beta)\gamma_0 \pm [(1-A^2)\gamma_0^2 k^2 + 4Agk]^{\frac{1}{2}}. \tag{12}$$

There is an additional branch to the dispersion relation, $\sigma = 0$, which is an artifact of the Lagrangian approach. It signals the ability to translate points along the interface without change of shape, and is usually termed a labelling mode. The result (12) is consistent with the results obtained by a linear analysis in the Eulerian frame (Kelvin 1871). We are unaware of any previous publication of the stability results in the Lagrangian frame for this problem, but the results may be obtained in a straightforward fashion.

The dispersion relation (12) has several features:

(i) The choice $\beta = -A$ in (12) removes the imaginary part of σ; i.e. it removes the translational component of σ. This fact provides additional justification for this choice of β in numerical calculations.

(ii) For $\gamma_0 \neq 0$, the real part of σ, which is the growth (or decay) rate of the linear modes, is proportional to $|k|$ for large k. This growth rate is an indication of Kelvin–Helmholtz instability.

(iii) For $\gamma_0 = 0$, the growth rate is proportional to $|k|^{\frac{1}{2}}$, for large k. This growth rate is an indication of Rayleigh–Taylor instability.

(iv) When $A = 1$, the Kelvin–Helmholtz instability does not occur even if $\gamma_0 \neq 0$. This reflects the fact that the Kelvin–Helmholtz instability is activated only when two fluids stream past each other.

The Kelvin–Helmholtz growth rate $\sigma(k) = |k|$ allows the possibility for singularity development. Consider a superposition of the linear growing modes in (11)

$$z(\alpha, t) = \alpha + \tfrac{1}{2}\beta\gamma_0 t + \sum_k a_k \, e^{\sigma(k)t} \, e^{ik\alpha}. \tag{13}$$

Assume that
$$|a_k| \sim c\, e^{-\kappa|k|}, \tag{14}$$

for large k, which corresponds to analytic initial data. Then at time t, the amplitude of the kth Fourier mode is of size $\exp\{-(\kappa - \gamma_0 t)|k|\}$. Decay of the Fourier components, and thus analyticity, is lost for $t = \kappa/\gamma_0$. This prediction by linear analysis of singularity formation for vortex sheets was first discussed by Birkhoff (1962) and since then much effort has been expended to verify that nonlinear effects do not prevent singularity development. Analytic studies by Moore (1979, 1985), Caflisch & Orellana (1986), and Duchon & Roberts (1988), and numerical studies by Meiron *et al.* (1982), Krasny (1986*b*) and Shelley (1992) all support the conclusion that singularities form in finite time. In particular, the calculations of Baker & Shelley (1990) and Shelley (1992) point out that it is the advection of vorticity along the sheet towards an accumulation point that signals the occurrence of singularities. Pugh (1989) was the first to show that these singularities also occur on free surfaces between immiscible liquids with different densities.

If $\gamma_0 = 0$, the argument based on linear analysis for singularity development fails. On the other hand, baronclinic generation of vorticity on the interface creates regions along the sheet where there is a mean level to the vortex sheet strength locally. Moreover, the region along the sides of the spikes contains vorticity advecting downwards from the bubble and upwards from the spike. The conditions are right for the nonlinear development of singularities. We show in this paper, by a simple analytic theory and by extensive computations, that singularities do occur.

3. The localized approximation

Siegel (1989) applied the ideas behind the approximate theory for vortex sheets, developed first by Moore (1979) and then extended by Caflisch *et al.* (1990), to the Rayleigh–Taylor instability. For completeness, we repeat the main points in the theory.

The approximation method is most easily described by extending the parameter α to be complex. The Rayleigh–Taylor equations are analytically extended to complex α as

$$\partial_t z^* = q^* + \beta\gamma/2z_\alpha, \tag{15a}$$

$$\partial_t \gamma = A\left[q_t^* z_\alpha + q_t z_\alpha^* - \frac{\beta\gamma}{2}\left(\frac{q_\alpha}{z_\alpha} + \frac{q_\alpha^*}{z_\alpha^*}\right) - \mathrm{i}g(z_\alpha - z_\alpha^*)\right] + \frac{A+2\beta}{4}\frac{\partial}{\partial\alpha}\left(\frac{\gamma^2}{z_\alpha z_\alpha^*}\right), \tag{15b}$$

in which

$$z^*(\alpha, t) = \overline{z(\bar{\alpha}, t)} \tag{16}$$

is the analytic extension of the conjugate function. In other words, z^* is an analytic function of α which equals $\bar{z}$ for real values of α. The complex velocity is given by

$$q^*(\alpha, t) = \frac{1}{2\pi\mathrm{i}}\mathrm{PV}\int_{-\infty}^{\infty} \frac{\gamma(\alpha+\zeta, t)}{z(\alpha, t) - z(\alpha+\zeta, t)}\mathrm{d}\zeta. \tag{17}$$

Decompose γ and z as

$$z(\alpha, t) = \alpha + s_+(\alpha, t) + s_-(\alpha, t) + s_0(t), \tag{18a}$$

$$\gamma(\alpha, t) = \gamma_+(\alpha, t) + \gamma_-(\alpha, t) + \gamma_0 \tag{18b}$$

in which s_+, γ_+ contain the positive wavenumber components of s, γ respectively and s_-, γ_- contain the negative wavenumbers, i.e.

$$s_+(\alpha, t) = \sum_{k>0} \hat{s}_k(t)\,\mathrm{e}^{\mathrm{i}k\alpha}, \quad s_-(\alpha, t) = \sum_{k<0} \hat{s}_k(t)\,\mathrm{e}^{\mathrm{i}k\alpha}, \tag{19a, b}$$

$$\gamma_+(\alpha, t) = \sum_{k>0} \hat{\gamma}_k(t)\,\mathrm{e}^{\mathrm{i}k\alpha}, \quad \gamma_-(\alpha, t) = \sum_{k<0} \hat{\gamma}_k(t)\,\mathrm{e}^{\mathrm{i}k\alpha}. \tag{19c, d}$$

The constant term in z is represented by $s_0(t)$, but it plays no role in the resulting equations. The constant term in γ is the mean vortex sheet strength γ_0, which we set to zero since our interest is in the classical Rayleigh–Taylor instability.

Note that

(i) The $*$-operator switches $+$components to $-$components, i.e.

$$(s^*)_+ = (s_-)^*, \quad (s^*)_- = (s_+)^*. \tag{20}$$

(ii) Since γ is real when α is real, $\hat{\gamma}_{-k} = \bar{\hat{\gamma}}_k$ so that

$$(\gamma_+)^* = \gamma_-. \tag{21}$$

The analytic equations (15) can be written as

$$z_t^* = I_1(z_\alpha, z_\alpha^*, \gamma, \gamma^*), \quad \gamma_t = I_2(z_\alpha, z_\alpha^*, \gamma, \gamma^*). \tag{22a, b}$$

The approximate theory is based on the following physical argument. Nonlinear interactions cause wavenumbers to add so that energy flows back and forth among

wavenumbers. However, the process of singularity development primarily involves flow of energy from low wavenumbers to high wavenumbers. Our approximation keeps this flow of energy to higher wavenumbers, but ignores all flow of energy from high to low wavenumbers. In other words, interactions of wavenumbers k_1 and k_2 to form wavenumber k_1+k_2 are neglected if $|k_1+k_2| < \max(k_1, k_2)$. This is equivalent to saying that interactions between positive k and negative k are neglected. Mathematically this is the same as retaining interactions of s_+ with s_+ and of s_- with s_-, but neglecting interactions of s_+ with s_-. For any function or operation $A[s]$, the approximation is then

$$A[s] \sim A[s_+] + A[s_-].$$

If s has a constant term, i.e. $s = s_+ + s_- + s_0$, the corresponding approximation is

$$A[s] \sim A[s_+ + s_0] + A[s_- + s_0] - A[s_0].$$

The neglected terms are just the interactions of s_+ and s_-.

We employ this approximation for both s and γ. Therefore (22) becomes

$$z_t^* = I_1(z_{\alpha+}, (z^*)_{\alpha+}, \gamma_+, (\gamma^*)_+) + I_1(z_{\alpha-}, (z^*)_{\alpha-}, \gamma_-, (\gamma^*)_-), \tag{23a}$$

$$\gamma_t = I_2(z_{\alpha+}, (z^*)_{\alpha+}, \gamma_+, (\gamma^*)_+) + I_2(z_{\alpha-}, (z^*)_{\alpha-}, \gamma_-, (\gamma^*)_-). \tag{23b}$$

The difference between (22) and (23) consists only of terms containing products of + and − components, such as

$$z_{\alpha+} z_{\alpha-}, \quad z_{\alpha+} \gamma_- \quad \text{or} \quad z_{\alpha+} (z^*)_{\alpha-}.$$

The advantage of this approximation is that now the integral in I_1 can be evaluated by a contour deformation, resulting in a purely local term coming from a residue. By using this evaluation, then taking + and − components of (23) and using $(\gamma^*)_- = \gamma_+$ we obtain the following system (for more details of the derivation see Appendix A):

$$\frac{\partial s_-^*}{\partial t} = \frac{\beta-1}{2} \frac{\gamma_+}{1+s_{\alpha+}}, \quad \frac{\partial s_+}{\partial t} = \frac{\beta+1}{2} \frac{\gamma_+}{1+s_{\alpha-}^*}, \tag{24a, b}$$

$$\frac{\partial \gamma_+}{\partial t} = \frac{A+\beta}{2} \frac{\partial}{\partial \alpha} \left(\frac{\gamma_+^2}{(1+s_{\alpha+})(1+s_{\alpha-}^*)} \right) - \mathrm{i}Ag(s_{\alpha+} - s_{\alpha-}^*), \tag{24c}$$

in which $s_-^* = (s_-)^* = (s^*)_+$. Mathematical analysis of (24) is simplified further if it is written as a quasi-linear system. Denote

$$\phi = 1 + s_{\alpha+}, \quad \psi = 1 + s_{\alpha-}^*, \quad \omega = \gamma_+, \tag{25}$$

and differentiate (24*a*, *b*) to obtain

$$\phi_t = \frac{\beta+1}{2} \frac{\partial}{\partial \alpha} \left(\frac{\omega}{\psi} \right), \quad \psi_t = \frac{\beta-1}{2} \frac{\partial}{\partial \alpha} \left(\frac{\omega}{\phi} \right), \tag{26a, b}$$

$$\omega_t = \frac{A+\beta}{2} \frac{\partial}{\partial \alpha} \left(\frac{\omega^2}{\phi\psi} \right) - \mathrm{i}Ag(\phi - \psi). \tag{26c}$$

The localized equations (26) are much simpler than the full equations (7) and (8), mainly in that they are purely local; i.e. they are differential equations rather than integro-differential equations. However, there is a defect to the approximate system

concerning the role of β. For the full equations (7) and (8), the solution for one choice of β is equivalent to the solution for any other choice of β; that is not the case for the approximate system. The source of this defect is simple. Different choices of β correspond to different parametrizations by α for the motion. The approximation involves Fourier transformation to make the decomposition into upper and lower analytic functions. Since changes of variables are not easily expressed through the Fourier transform, there is no simple relation between solutions of the approximate system for different choices of β. Nevertheless, we can establish that the solutions for various β are asymptotically close to the exact solution when the deformations of the interface are small and the singularities are far from the real axis (Siegel 1989; S. J. Cowley, private communication). Consequently, the nature of the singularities are predicted reliably by the approximate system independently of β. Some evidence for the generic nature of the singularities is given in §6.

The approximate system (26) is a first-order system with the characteristic speeds

$$\lambda_1 = 0, \tag{27a}$$

$$\lambda_2 = (-(A+\beta)+\mathrm{i}[1-A^2]^{\frac{1}{2}})\frac{\omega}{2\phi\psi}, \tag{27b}$$

$$\lambda_3 = (-(A+\beta)-\mathrm{i}[1-A^2]^{\frac{1}{2}})\frac{\omega}{2\phi\psi}. \tag{27c}$$

These characteristics speeds are complex in general, and so information can move towards the real α-axis and reach it in finite time. Baker (1990) shows diagrams of the characteristics for the Kelvin–Helmholtz instability and, in particular, he confirms that the motion of singularities may be described as the envelop of breaking characteristics as predicted by Moore (1985). Note that the characteristic speeds are proportional to ω so that as vorticity is created baronclinically, information moves with increasing speed towards the real α-axis. We will construct solutions that have singularities which move with constant speed towards the real α-axis and reach it at some time t_c, at which time a curvature singularity appears on the fluid interface.

As expected, the linearized version of (26) has the same dispersion relation as (12). The characteristic speeds λ are the limiting phase speeds $\lambda = \lim_{k\to\infty} \sigma(k)/k$. Note that (12) is purely real when $\beta = -A$; in other words the choice $\beta = -A$ puts the system in a natural moving frame.

Furthermore, at $A = 1$, and $\beta = -1$ the localized approximation equations simplify to a linear system,

$$\phi_t = 0, \quad \psi_t = -\frac{\partial}{\partial\alpha}\left(\frac{\omega}{\phi}\right), \quad \omega_t = -\mathrm{i}Ag(\phi-\psi). \tag{28a–c}$$

In particular ϕ is independent of time and is thus known from the initial data. The remaining equations for ψ and ω are then linear, with coefficients that depend on α. An obvious consequence is that there is no singularity development in (ϕ, ψ, γ) for α in the complex plane when ϕ is constant and the initial data are entire. If there are singularities in the lower half-plane, then it can be shown from (28) that these singularities do not move toward the real α-axis and consequently are not physically realized.

4. Travelling wave solutions

We follow previous studies of singularity formation on vortex sheets by seeking solutions that are 2π-periodic in space. A class of exact solutions to the localized equations (26) which take the form of periodic travelling waves in the complex plane was found by Siegel (1989). The solutions are significant since they provide explicit information about singularity formation in the localized approximation equations. Consequently, the need for a second asymptotic analysis like that employed by Moore (1979) is unnecessary.

The travelling wave solutions can most easily be obtained by looking for solutions to (26) of the form $\phi = \phi(\xi)$, $\psi = \psi(\xi)$ and $\omega = \omega(\xi)$ with ξ defined by $\xi = \mathrm{i}(\alpha + \sigma t)$. Substitution of these forms into (26) gives the following system of ODEs:

$$\sigma\phi_\xi = \frac{\beta+1}{2}\frac{\partial}{\partial\xi}\left(\frac{\omega}{\psi}\right), \tag{29a}$$

$$\sigma\psi_\xi = \frac{\beta-1}{2}\frac{\partial}{\partial\xi}\left(\frac{\omega}{\phi}\right), \tag{29b}$$

$$\sigma\omega_\xi = \frac{A+\beta}{2}\frac{\partial}{\partial\xi}\left(\frac{\omega^2}{\phi\psi}\right) - Ag(\phi-\psi). \tag{29c}$$

The first two equations can be integrated directly, yielding

$$\phi = \phi(0) + \frac{\beta+1}{2\sigma}\left(\frac{\omega}{\psi} - \frac{\omega(0)}{\psi(0)}\right), \tag{30a}$$

$$\psi = \psi(0) + \frac{\beta-1}{2\sigma}\left(\frac{\omega}{\phi} - \frac{\omega(0)}{\phi(0)}\right). \tag{30b}$$

By the definitions (25), the constant part in the Fourier expansions for both ϕ and ψ is equal to one, whereas there is no constant part in the Fourier expansion of ω. Consequently, the right-hand sides of (30) must have a mean value of 1, and this implies that following relationships must hold:

$$\phi(0) - \frac{\beta+1}{2\sigma}\frac{\omega(0)}{\psi(0)} = 1, \quad \psi(0) - \frac{\beta-1}{2\sigma}\frac{\omega(0)}{\phi(0)} = 1.$$

With these values, (30) becomes

$$\phi = 1 + \frac{1+\beta}{2\sigma}\frac{\omega}{\psi}, \quad \psi = 1 - \frac{1-\beta}{2\sigma}\frac{\omega}{\phi}. \tag{31a, b}$$

In order to integrate (29*c*), we use (31) to express ϕ and ψ in terms of $\Omega = \omega/\sigma$;

$$2\phi = 1 + \Omega + [1 + 2\beta\Omega + \Omega^2]^{\frac{1}{2}}, \quad 2\psi = 1 - \Omega + [1 + 2\beta\Omega + \Omega^2]^{\frac{1}{2}}. \tag{32a, b}$$

Here the branch of the square root is also selected by the requirement that the constant parts in the expansions of ϕ and ψ equal one. Upon substituting (32) into (29*c*) we obtain

$$\Omega_\xi = (A+\beta)\frac{\partial}{\partial\xi}\left(\frac{\Omega^2}{1 + \beta\Omega + [1 + 2\beta\Omega + \Omega^2]^{\frac{1}{2}}}\right) - \frac{Ag}{\sigma^2}\Omega. \tag{33}$$

As we have pointed out earlier, the choice $\beta = -A$ selects a convenient parametrization, and here we find that this choice allows a closed-form solution for (33). The more difficult analysis for $\beta \neq -A$ will be given in §6. For $\beta = -A$, the resulting equation is $\Omega_\xi = -(Ag/\sigma^2)\Omega$. The requirement that Ω is upper analytic and 2π-periodic in α forces $Ag/\sigma^2 = -n$ for integer n. We choose $n = 1$, resulting in the solution

$$\omega = \omega(0)\,e^{\xi}, \quad \sigma = \pm i(Ag)^{\frac{1}{2}}, \tag{34a,b}$$

where $\omega(0)$ is the complex amplitude. The speed of the travelling wave is in the imaginary α-direction, and corresponds to a growing mode in the linear analysis.

Surprisingly, the speed of the nonlinear travelling wave solution is independent of the amplitude and is identical to the speed given by a linear analysis. It can be shown that this is a general property of periodic travelling wave solutions to upper analytic systems of PDEs, under the condition that the system of ODEs resulting from the substitution of the travelling wave variable is autonomous.

Several properties of the travelling wave solutions (32), (34) are immediately apparent. One is that these solutions contain exclusively growing or decaying modes depending on whether the sign of $\mathrm{Im}\,(\sigma)$ is negative or positive, respectively. Obviously, we shall be interested in the behaviour of the growing modes, so $\sigma = -i(Ag)^{\frac{1}{2}}$. These solutions also correspond to a special choice of initial condition for the sheet position and sheet strength given by

$$x_\alpha = 1 + \mathrm{Re}\,\{s_{\alpha+} + s_{\alpha-}\} = \mathrm{Re}\,\{[1 + 2A\eta + \eta^2]^{\frac{1}{2}}\}, \tag{35a}$$

$$y_\alpha = \mathrm{Im}\,\{s_{\alpha+} + s_{\alpha-}\} = -\mathrm{Im}\,\{\eta\}, \tag{35b}$$

$$\gamma = 2\,\mathrm{Re}\,\{\omega\} = 2\,\mathrm{Re}\,\{-\sigma\eta\}, \tag{35c}$$

where $\eta = -(\omega(0)/\sigma)\exp(i\alpha)$. Notice, in particular, that $y = H - (\omega(0)/\sigma)\cos(\alpha)$, so that $\omega(0)/\sigma$ is a measure of the amplitude of the initial perturbation. We choose $-\omega(0)/\sigma = \epsilon$ to be real, so that the rising bubble of lighter fluid is centred at $\alpha = 0$ and the falling spike of heavier fluid at $\alpha = \pi$. The parameter H is chosen so that the interface has zero mean height;

$$\int_0^{2\pi} (H + \epsilon\cos(\alpha))\,\mathrm{Re}\,\{[1 + 2A\,e^{i\alpha} + e^{2i\alpha}]^{\frac{1}{2}}\}\,d\alpha = 0. \tag{36}$$

The nature of the singularity is easily deduced from the travelling wave solution (32) and (34). We deal first with the case $A \neq 1$. While ω remains analytic for all time, ϕ and ψ have square-root singularities whenever $\omega/\sigma = A \pm i[1 - A^2]^{\frac{1}{2}}$. Since $\omega = -\epsilon\sigma e^{\xi}$, we find that the singularities move along the straight lines

$$\alpha = i(Ag)^{\frac{1}{2}}t - i\ln(-A \pm i[1 - A^2]^{\frac{1}{2}}) + i\ln\epsilon \tag{37}$$

in the complex α-plane, and reach the real axis at positions corresponding to

$$\alpha_c = \pi \pm \tan^{-1}([1 - A^2]^{\frac{1}{2}}/A), \tag{38}$$

and at time

$$t_c = \frac{1}{(Ag)^{\frac{1}{2}}}\ln\frac{1}{\epsilon}. \tag{39}$$

Notice that when $\epsilon < 1$, the singularities lie below the real axis, which is consistent with the assumption that ϕ and ψ are analytic in the upper half-plane, and that they move vertically upwards until they reach the real axis at α_c.

In terms of the physical variables, the solution takes the form of (35) but where $\eta = \epsilon \exp(i\alpha + (Ag)^{\frac{1}{2}} t)$. The singularities in x occur as two complex-conjugate pairs, lying on either side of π. There are no singularities in y or γ. The fact that x_α has a square-root singularity at t_c indicates that $x_{\alpha\alpha} \to \infty$ and consequently the curvature will blow up. A simple calculation of the curvature $\kappa = (x_\alpha y_{\alpha\alpha} - y_\alpha x_{\alpha\alpha})(x_\alpha^2 + y_\alpha^2)^{-\frac{3}{2}}$ shows that $\kappa \sim |t - t_c|^{-\frac{1}{2}}$ for $\alpha = \alpha_c$ and $\kappa \sim |\alpha - \alpha_c|^{-\frac{1}{2}}$ for $t = t_c$.

Another quantity of interest is the vortex sheet strength $\tilde{\gamma} = \gamma/(|z_\alpha|)$. This quantity remains bounded in α for all Atwood numbers. Moreover, for $A < 1$,

$$\tilde{\gamma}_\alpha = -\gamma \frac{x_\alpha x_{\alpha\alpha} + y_\alpha y_{\alpha\alpha}}{(x_\alpha^2 + y_\alpha^2)^{\frac{3}{2}}} + \frac{\gamma_\alpha}{x_\alpha^2 + y_\alpha^2}$$

remains bounded at the singularity positions given by (38), since, although $x_{\alpha\alpha} \to \infty$ at these positions, $x_\alpha \to 0$ such that $x_\alpha x_{\alpha\alpha}$ remains bounded. However, $\tilde{\gamma}_{\alpha\alpha} \to \infty$ at these singularities.

Now we take note of the positioning for the trajectories of the singularities in the complex α-plane. When $A = 0$, the trajectories lie along the lines $\alpha = \frac{1}{2}\pi$ and $\alpha = \frac{3}{2}\pi$. This case has been studied before by Pugh (1989) in the Boussinesq limit. For $0 < A < 1$, the trajectories lie symmetrically on either side of $\alpha = \pi$, and the larger A is, the closer to $\alpha = \pi$ they occur. In terms of physical variables, the location of the curvature singularities at $t = t_c$ is symmetrically on either side of the tip of the spike. As $A \to 1$, the singularities get closer to the spike tip.

When $A = 1$, the trajectories coalesce and cancel. The mathematical nature of the singularity cancellation is clearly seen from (32). At $A = 1$ (and $\beta = -A$) the equations (32) for ϕ and ψ become

$$2\phi = 1 + \Omega + [(1-\Omega)^2]^{\frac{1}{2}} = 2,$$
$$2\psi = 1 - \Omega + [(1-\Omega)^2]^{\frac{1}{2}} = 2 - \Omega,$$

and the square-root singularity is removed. This is a solution to the $A = 1$, $\beta = -1$ system (28) in the special case that $\phi(\alpha, t) = \phi(\alpha, 0) = 1$. Note that this solution is linear in the sense that it satisfies a linear system with constant coefficients and therefore contains only wavenumbers present in the initial perturbation. However, this solution is nonlinear in the Eulerian sense since a mode in the Lagrangian parameter α does not correspond to a perturbation that is sinusoidal in x, y space.

From (35), we have for $A = 1$

$$z_\alpha = x_\alpha + iy_\alpha = 1 + \epsilon \exp g^{\frac{1}{2}} t\, e^{-i\alpha}. \tag{40}$$

While z remains analytic in α, there is a failure in the conformal map from α to z since z_α vanishes along the line (37). Note that this singularity would be observable if we consider the arclength as a complex variable instead of α. In fact, when $t = -(\log \epsilon)/g^{\frac{1}{2}}$ and α near π, $x_\alpha \sim \frac{1}{2}(\alpha - \pi)^2$ and $y_\alpha \sim (\alpha - \pi)$ so that $y \sim (\frac{9}{2})^{\frac{1}{3}}(x - \pi)^{\frac{2}{3}}$ locally near the tip of the Rayleigh–Taylor spike. This geometric singularity in the travelling wave solution (32) of the localized approximation equations with $A = 1$ differs from the singularities for $A < 1$. For example, the curvature blows up differently, having behaviour $\kappa \sim (t - t_c)^{-2}$ for $\alpha = \alpha_c = \pi$ and $\kappa \sim (\alpha - \pi)^{-1}$ for $t = t_c$. The derivative of the vortex sheet strength $\tilde{\gamma}$ blows up at the singularity. On the other hand the numerical results presented in the next section show that this geometric singularity does not occur in solutions of the full equations. The nonlinear terms neglected in the asymptotic analysis slow down the approach of the zero in z_α to the real axis.

5. Numerical results

The behaviour of the solutions to the approximate equations gives precise predictions on the formation of singularities on the interface in finite time. In this section, numerical calculations are performed to verify these predictions and test the validity of the approximate equations. The agreement is remarkably good for values of A not near one, but we find a divergence in the behaviour of the numerical solutions from those predicted by the approximate equations for $A \to 1$. The results show that the speed by which the singularities approach the real axis slows down when A is near 1, and they may not reach the real axis in finite time when $A = 1$. Since it is very difficult to calculate the numerical solution close to the singularity time, such conclusions are not absolutely certain, and so we have reported the results for both the asymptotic model and the full simulations as an encouragement for further study.

Equations (7), (8) may be rewritten in terms of the dipole sheet strength μ, which satisfies $\mu_\alpha = \gamma$; see Baker *et al.* (1982) for details. The calculation of the complex potential, Φ, parallels (9):

$$\Phi(\alpha, t) = \frac{1}{2\pi \mathrm{i}} \mathrm{PV} \int \frac{\mu(\alpha', t)\, z_\alpha(\alpha', t)}{z(\alpha, t) - z(\alpha', t)} \mathrm{d}\alpha'. \tag{41}$$

The complex velocity is given by $\bar{q} = \Phi_\alpha / z_\alpha$. The motion of the interface is governed by

$$\bar{z}_t = \bar{q} + \beta\gamma / 2 z_\alpha. \tag{42}$$

The evolution of the dipole sheet strength is given by

$$\mu_t = 2A \left[\mathrm{Re} \left\{ \Phi_t - \frac{\beta\gamma q_\alpha}{2 z_\alpha} \right\} - \tfrac{1}{2} q \bar{q} + g \,\mathrm{Im}\{z_\alpha\} \right] + \frac{A + 2\beta}{4} \frac{\partial}{\partial \alpha} \left(\frac{\gamma^2}{|z_\alpha|^2} \right). \tag{43}$$

This alternative form for the equations offers several computational advantages, and has been used successfully to study several different free-surface flow problems (Baker 1983; Baker, Meiron & Orszag 1984; Baker *et al.* 1987; Baker & Moore 1989). The numerical method used to solve the equations is essentially the same as in these previous studies, so we provide just a short summary of it.

At some time t, we assume that we know the location of the free surface and the dipole sheet strength at equally spaced points in α. Derivatives of z are found by the use of quintic splines. In fact, all differentiation is performed numerically through the use of quintic splines. The complex potential along the interface is calculated by the use of an alternate point trapezoidal rule (see Baker 1983) to approximate (41), and the complex velocity is obtained by differentiating the complex potential. The evolution equation for the dipole strength is then solved by iteration; the solution is considered converged when the absolute difference in the iterates is less than 10^{-18}. By knowing the velocity at the interface and the rate of change of the dipole strength, we can update the position of the interface and the dipole strength through a standard solver. In particular, we use the fourth-order Adams–Moulton predictor-corrector. The initial condition (35) must be integrated in order to specify both the initial position of the interface and the dipole strength. The integrands are represented by a truncated Fourier series and then integrated analytically. Details are available in Appendix B.

5.1. $A < 1$

Since the motion of the interface is susceptible to the Kelvin–Helmholz instability, small perturbations, in particular those introduced as a consequence of round-off errors, grow very rapidly and soon destroy the accuracy of the calculation.

Consequently, we employ the spectral filtering technique of Krasny (1986*b*) at each time step to suppress the rapid growth of round-off errors. However, even in double precision on a CRAY-YMP computer, the number of expressions that must be evaluated drives up the round-off error so that we could not set it as low as Shelley (1992) could for his detailed study of the singularity formation on a vortex sheet undergoing Kelvin–Helmholz instability. Unfortunately, the higher the spatial resolution of our calculations, the higher the filter level must be set. We kept the filter level as low as possible to get accurate results close enough to the singularity time so that we could make useful comparisons with asymptotic theory. For the resolutions given by $N = 128$, $N = 256$ points along the interface, the lowest value that the filter level could be set is 10^{-18}, 10^{-16} respectively. With a time step of 0.00625 $(Ag)^{-\frac{1}{2}}$, numerically generated profiles of the interface shown in this paper have an accuracy of at least 10^{-7}.

In figure 1, we show the profiles of the interface as calculated by several methods for three choices of the Atwood number. The equations of motion preserve the symmetry $x(-\alpha) = x(\alpha)$ and $y(-\alpha) = y(\alpha)$, so that only one half of a symmetric wave pattern needs to be shown. In the first column we show the predictions of linear theory conducted in the Eulerian frame, and of linear theory conducted on (7), (8), in other words, in a Lagrangian frame. The right-hand plots contain the predictions of the aysmptotic theory of this paper and the results of the numerical calculations. All the profiles use (35), (37) as an initial condition with $\epsilon = 0.1$. Details of the calculations for the profiles based on linear and asymptotic theory are available in Appendix B. The profiles are shown at time $t = 2.0\,(Ag)^{-\frac{1}{2}}$; asymptotic theory predicts singularity formation at $t_c = 2.3\,(Ag)^{-\frac{1}{2}}$. The linear theories show the overall trend in the profile, but agreement is not quantitative nor do the linear theories predict singularity formation. The asymptotic theory is very good for the range $0 < A < 0.9$, but, as we show later, the agreement deteriorates as $A \to 1.0$. Note further that the profiles are shown quite close to the time of singularity formation, but they show no strong variation in height. The Kelvin–Helmholtz singularity occurs as a consequence of vorticity accumulation along the interface.

We turn now to the major part of our numerical study, the detection of singularities in the complex α-plane of the full solutions to (42), (43). We assume that the singularity closest to the real axis has the form,

$$x(\alpha) = (\alpha - \alpha_r + i\delta)^{\nu + i\tau} f_1(\alpha) + (\alpha - 2\pi + \alpha_r + i\delta)^{\nu - i\tau} f_2(\alpha), \tag{44}$$

where $f_1(\alpha)$ and $f_2(\alpha)$ are analytic in the neighbourhood of the singularities. We have placed the singularities symmetrically about $\alpha = \pi$ as required by the symmetry of the initial conditions. This assumption dictates that the singularities will occur on either side of the spike. Also, we show the position and nature of the singularities in the lower half-plane; there will be a corresponding pair in the upper half-plane. The singularity pair in the lower half-plane influences the coefficients in the Fourier series for x,

$$x(\alpha) = p + \sum_k a_k e^{ik\alpha}, \tag{45}$$

for positive k values. In fact, for large k,

$$a_k \sim \frac{ia}{k^{\nu+1}} e^{-\delta k} \sin(k\alpha_r + \tau \ln k + \phi), \tag{46}$$

where a, ϕ are two real constants related to the strength and phase of the singularity. This form for the Fourier transform was also used by Pugh (1989).

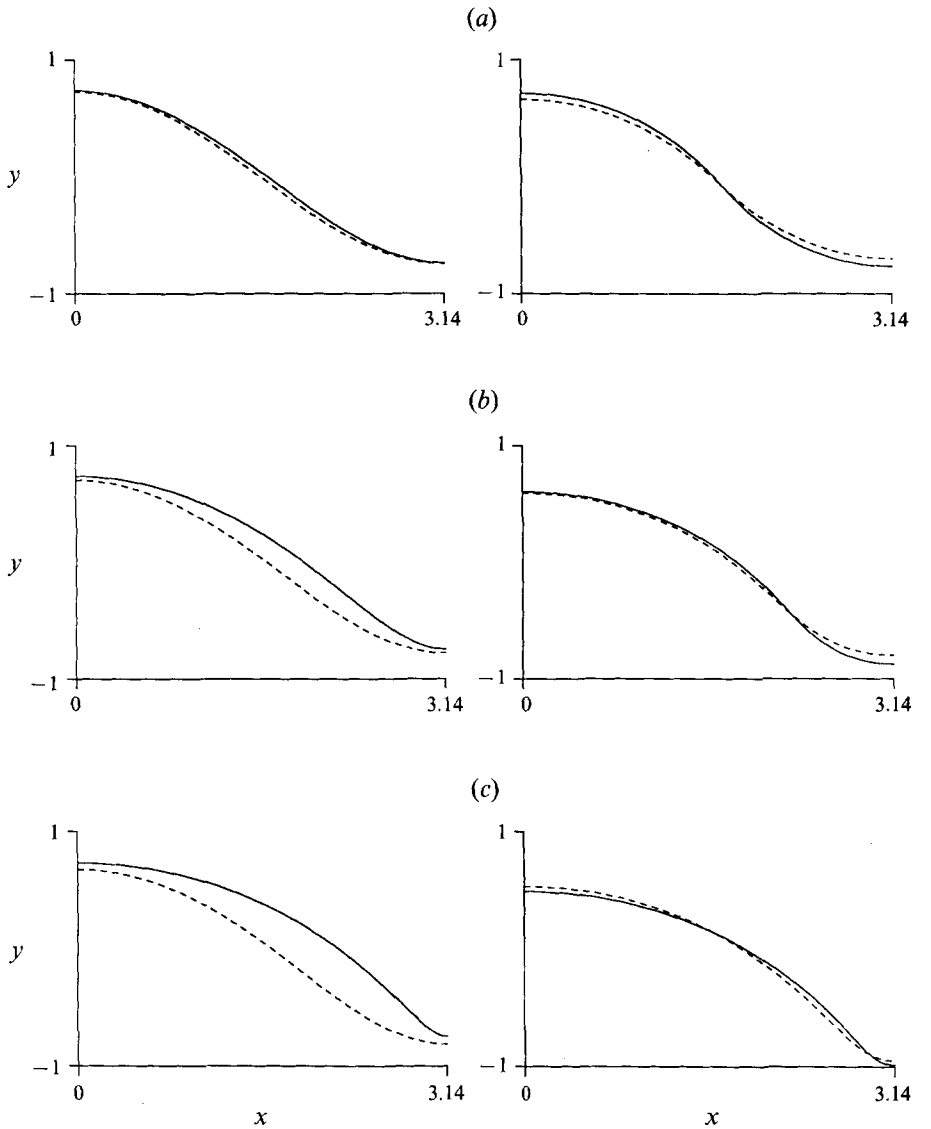

FIGURE 1. A comparison of the interfacial profiles determined by linear theories, our asymptotic theory, and numerical simulations, for (*a*) $A = 0.1$, (*b*) $A = 0.5$, (*c*) $A = 0.9$. Only half of the periodic pattern is shown. The left-hand profile for each choice of A shows the results of a Lagrangian linear stability analysis (solid) and an Eulerian linear stability analysis (dashed). The right-hand profiles give the results of the numerical simulation (solid) and our asymptotic theory (dashed). All profiles are shown at $t = 2.0(Ag)^{-\frac{1}{2}}$.

Numerical solution to (42) and (43) provides discrete points z_j representing the location of the interface and discrete values μ_j of the dipole sheet strength at these points. Standard fast-Fourier-transform methods may be used to get approximate Fourier coefficients. We seek a form fit of the numerically determined Fourier coefficients with (46) by techniques similar to those used by Pugh (1989) and Pugh & Cowley (1993). We take six sequential values of the numerical Fourier coefficients, $\tilde{a}_{k-5}, \tilde{a}_{k-4}, \tilde{a}_{k-3}, \tilde{a}_{k-2}, \tilde{a}_{k-1}, \tilde{a}_k$, say, where $\tilde{a}_k = \mathrm{Im}\{a_k\}$, and equate them to the form in (46) to generate six equations for the unknowns, a, ϕ, α_r, δ, ν, and τ. We solve these

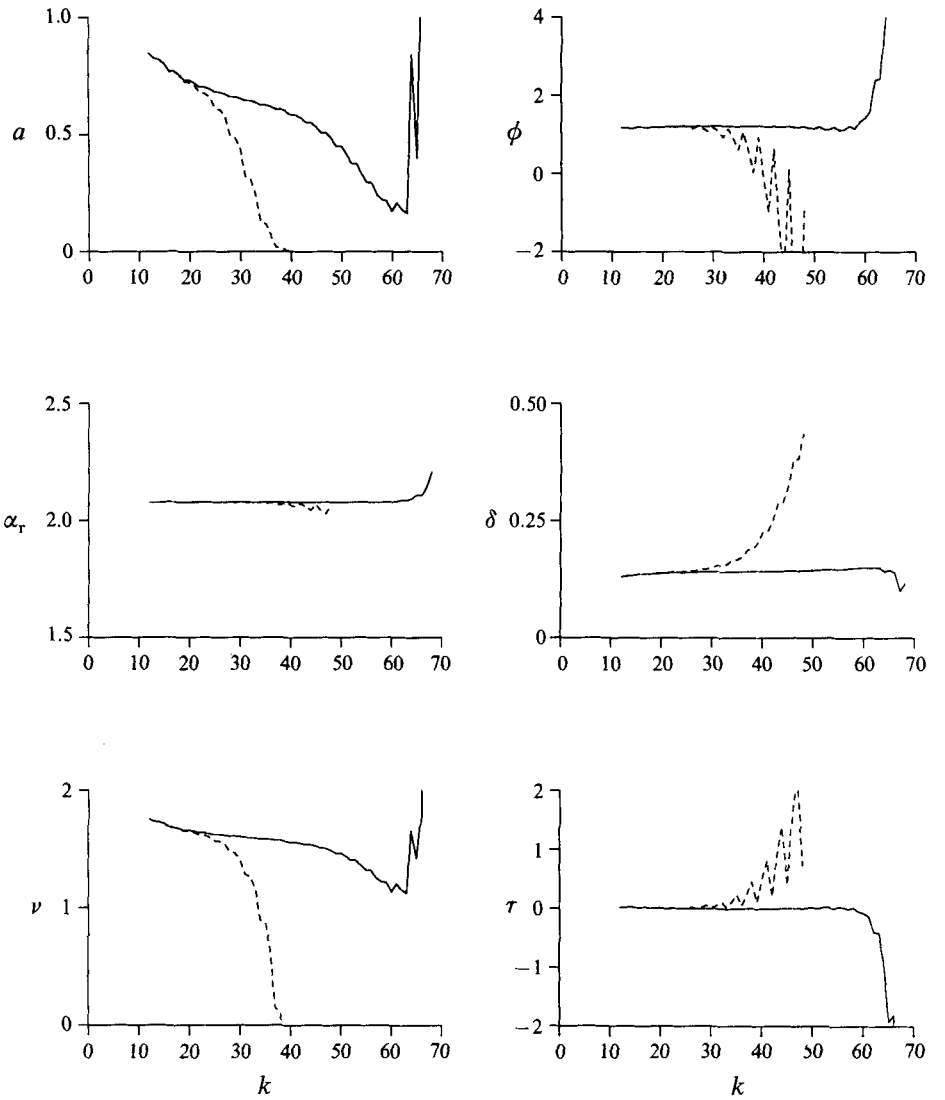

FIGURE 2. Variation of the parameters in the form fit to (45), performed locally on the Fourier coefficients of $x(\alpha)$. The data are taken from numerical simulations with $N = 128$ points (dashed) and $N = 256$ points (solid). The results are shown for $A = 0.5$ at time $t = 2.1875(Ag)^{-\frac{1}{2}}$.

equations by Newton's method. The solution is considered a local fit and labelled with the index k. In this way, we generate profiles for the coefficients in the form fit as k is varied.

Of course we need good starting guesses for the coefficients in the form fit in order for Newton's method to converge. For $A = 0.1$, and at time $t = 1.9(Ag)^{-\frac{1}{2}}$, we use a variety of approximations in order to get the first data to converge, including local fits to simpler forms, least-squares fits and adjustments by hand on graphical output. This process leads to initial guesses for the coefficients that converge under Newton iterations. Pugh (1989) also experienced difficulty in obtaining good first guesses. He used different methods to get Newton's method to converge. Once a solution has been found for a certain A and certain t, embedding may be employed to obtain solutions

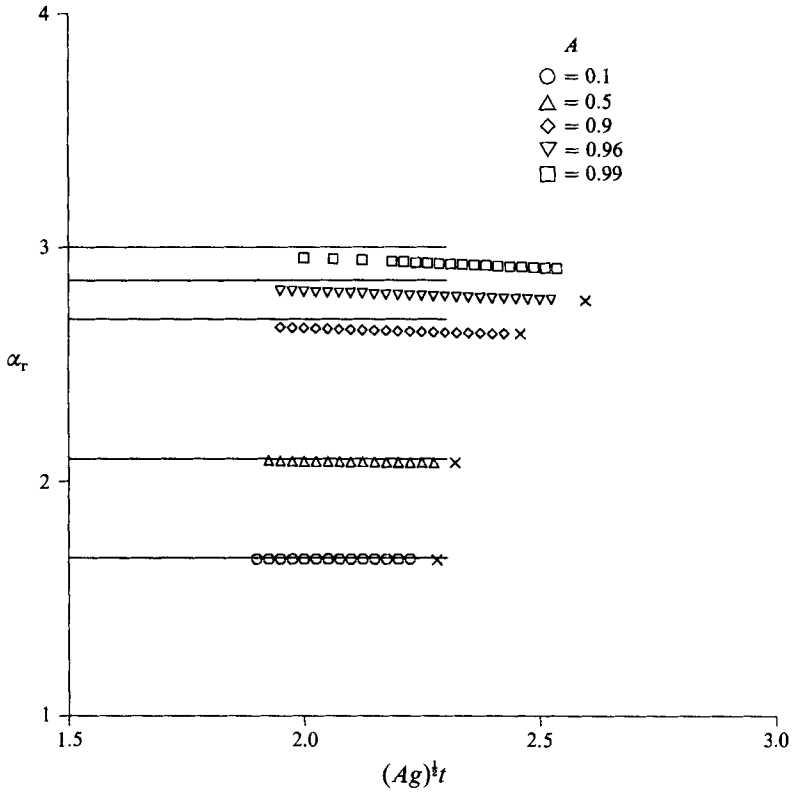

FIGURE 3. The real part, α_r, of the singularity trajectory for various A as a function of time, $(Ag)^{\frac{1}{2}}t$. The solid lines up to $t_c = 2.3(Ag)^{-\frac{1}{2}}$ are the predictors of asymptotic theory. The symbol × is the extrapolated value at the singularity time determined numerically.

for other values of A and t. In particular, for each A, we use the results of the previous time level to give the first guesses in Newton's methods for the current time level. Similarly, for a new value of A, we use the data from the previous value of A as a first guess. Thus we are able to generate profiles of the coefficients determined locally over six adjacent values of k at fixed values of A and t.

In figure 2, we show how the coefficients of the form fit vary typically with k for two different spatial resolutions. Following Pugh (1989), we find this approach more useful in assessing the form fit than an approach based on nonlinear least-squares fit covering a range in k. Spatial resolution is the most important factor in revealing the asymptotic form of the Fourier coefficients. Increasing the filter level by two orders of magnitude, or doubling the timestep, make no changes to the profiles in figure 2. Four of the profiles show clear tendencies of being constant at large values of k before errors contaminate the results. In particular, the position of the singularity, $\alpha_r - i\delta$, is determined quite reliably. Since τ appears to be zero, the singularity is a branch point with a real exponent. Unfortunately, the value of this exponent is not determined reliably. Higher resolution is needed, but the computer costs became prohibitive. Both the amplitude, α, and the exponent, ν, show a decay to constant values, similar to that observed by Pugh (1989) and Shelley (1992) in their studies of singularities in vortex sheet motion. Our asymptotic theory predicts the motion of branch point singularities with $\nu = 1.5$. The decay in ν is certainly consistent with this prediction. However, the

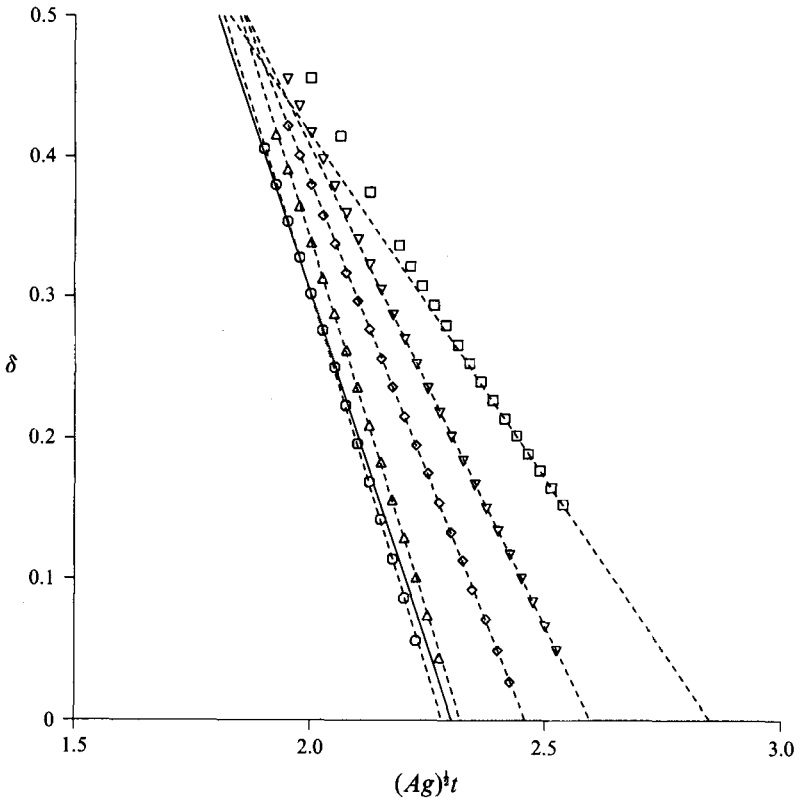

FIGURE 4. The imaginary part, δ, of the singularity trajectory for various A as a function of time, $(Ag)^{\frac{1}{2}}t$. The solid line is the prediction from asymptotic theory. The dashed lines are a linear least-squares fit to the numerical results. Symbols as figure 3.

asymptotic theory with the special travelling waves predicts a singularity in $x(\alpha, t)$ only. In fact, we find companion singularities in both $y(\alpha, t)$ and $\gamma(\alpha, t)$ that occur in the same place in the complex α-plane, but they have amplitudes that are much lower. It seems reasonable to interpret them as depending parasitically on the singularity in $x(\alpha, t)$.

As a result of the form fit, we obtain a good approximation to the location of the singularity by taking the average value of α_r and δ over a range of k. For $A = 0.5$, shown in figure 2, the range we choose is $30 \leqslant k \leqslant 40$. Slightly different ranges for other values of A are sometimes used, depending on the appearance of the profiles corresponding to figure 2. Consequently, we are able to track the singularity in time for various A. However, practical considerations impose some constraints. The singularity must be close enough to the real axis of α so that sufficient Fourier coefficients have values above the filter level. Since the amplitude in the form fit (46) is $O(1)$, we must have $e^{\delta k} > k^{2.5} \times 10^{-18}$, where we assume $\nu = 1.5$ and we set the filter level at 10^{-18}. For the first 30 or 50 Fourier coefficients to be above the filter level, we must have $\delta < 1.1$ or $\delta < 0.6$ respectively. On the other hand, when the singularity is very close to the real axis, the location of the interface and the dipole sheet strength develop small-scale oscillations which prevent convergence in the iterative solution of (43).

In figures 3 and 4, we show the real and imaginary parts of the trajectory of the singularity for various A. Asymptotic theory predicts that the real part of the trajectory should remain constant in time. These constants are drawn as solid lines in figure 3 up

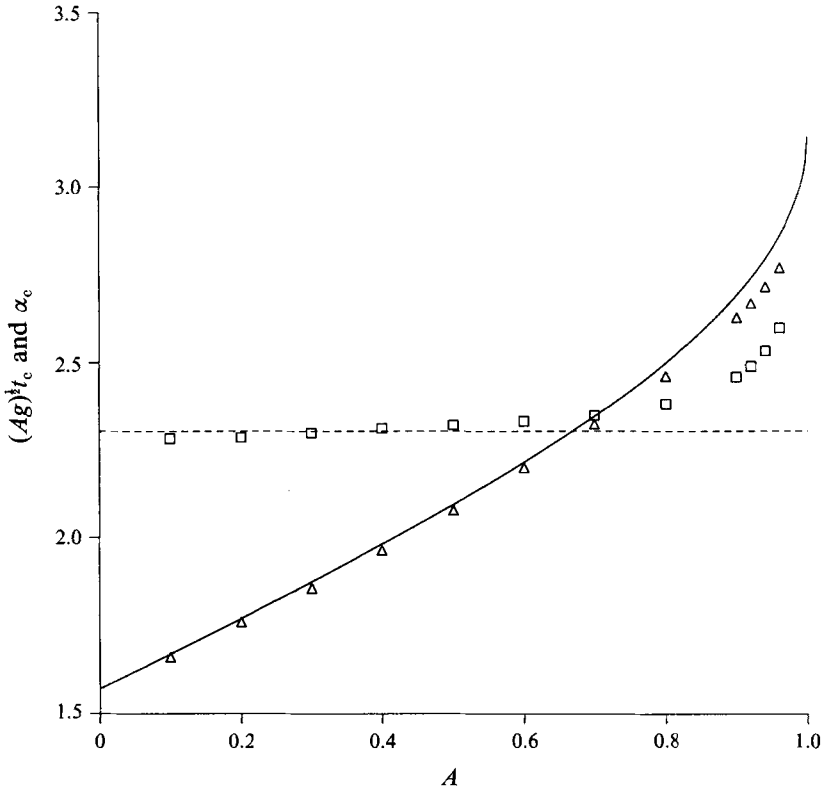

FIGURE 5. Estimates from the numerical calculations for singularity time, t_c (squares), and the location on the real axis, α_c (triangles), compared to predictions from asymptotic theory. The dashed curve gives the prediction for t_c, the solid curve for α_c.

to the critical time $t_c = 2.3(Ag)^{-\frac{1}{2}}$ predicted by asymptotic theory. The numerical results show that the real parts of the trajectory are almost constant, but have a slight tendency to move away from the spike tip at $\alpha = \pi$.

In figure 4, the approach of the singularity to the real axis is shown by a time sequence of symbols for several values of A. The solid straight line is the prediction from asymptotic theory for all A. For values of A close to 1, we observe a tendency in the trajectories to slow down as they approach the real axis. When the singularities are more than 0.5 away from the real axis, then the trajectories are close to asymptotic prediction. The dashed lines show a least-squares fit to a straight line. For $A \leqslant 0.9$, the fit is over all the data shown, but for $A = 0.96$ and 0.99, the fit is only over the closest six points to the real axis. For $A \leqslant 0.96$, the close fit of the straight lines to the data indicate strongly that the singularity will hit the real axis at a time that can be estimated by extrapolation. Extrapolated values of the location on the real axis where the singularity will occur are also shown in figure 3 as an $\times$ at the end of each time sequence. Unfortunately, we are unable to continue the calculations for $A = 0.99$ for later times. The interface forms a long thin spike and we need more points to resolve its motion. We make no attempt to estimate t_c for this case.

We have conducted a range of calculations for various A. In each case we determine extrapolated values for the times, t_c, at which the singularities reach the real axis at positions, α_c. In figure 5, we show how t_c and α_c vary with A, except that we give no results for $A > 0.96$ since we are unable to run our calculations long enough. Also

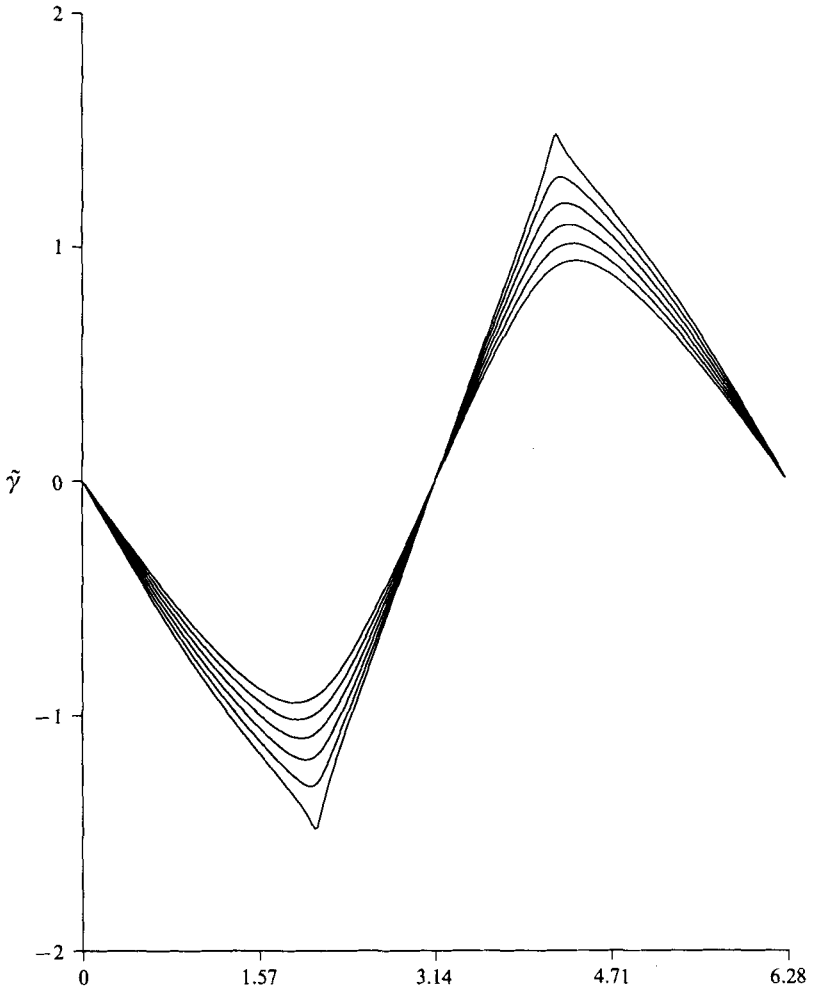

FIGURE 6. Profiles of the vortex sheet strength for $A = 0.5$ at times $(Ag)^{\frac{1}{2}}t = 1.925$, 2.000, 2.075, 2.150, 2.225, 2.300. Profiles with increasing amplitudes correspond to later times.

shown are the predictions of asymptotic theory. The predictions are very good for small values of A. The loss in accuracy at larger values of A is related to the more deformed profile of the interface when the singularity reaches the real axis. The interaction between modes in the Fourier spectrum of opposite sign in wavenumbers are no longer negligible.

In figure 6, we show the vortex sheet strength, $\tilde{\gamma}$, along the sheet for a sequence in time shortly before the singularity formation. We choose $A = 0.5$, but this case is representative. The vortex sheet strength is forming two cusps, consistent with the asymptotic theory, and similarly to those found in vortex sheets.

5.2. $A = 1$

When $A = 1$, we are able to run our code without the need for the spectral filter. Eventually, lack of resolution terminates the code. In agreement with the asymptotic theory, no singularity was detected near $\alpha_r = \pi$ during the times for which the calculations could be done. On the other hand, the maximum curvature, as shown in

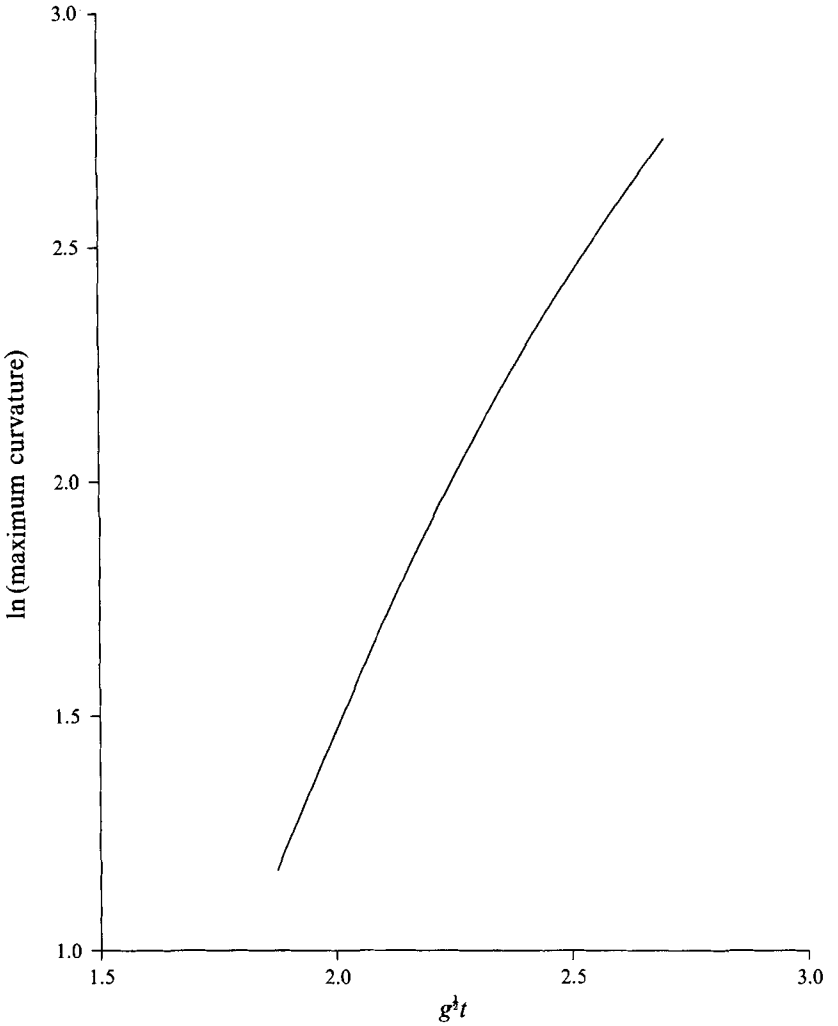

FIGURE 7. The growth in the logarithm of the maximum curvature ($\alpha = \pi$).

figure 7, grows less slowly than exponential. Examination of the spectrum for the curvature shows that the zero in z_α approaches (40), but does not reach the real axis in finite time.

The absence of singularities when $A = 1$ is explained in the asymptotic theory as a coalescence and annihilation of the singularity trajectories (37). This effect is a consequence of the choice $\beta = -A$ in the travelling wave solutions. The question arises as to the behaviour of the singularities if they are present in the initial conditions when $A = 1$. The next section considers this case specifically.

6. Additional travelling wave solutions

The travelling wave solutions for the approximate system were found explicitly under the choice $\beta = -A$ in §4. In this section additional travelling waves are analysed for other values of β. For $\beta \neq -A$, we must solve (33) to determine the travelling wave solution. As remarked earlier, the speed of the travelling wave is identical to the speed given by a linear analysis. When ω is small, (33) can be written as $\sigma^2\omega_\xi = -Ag\omega + O(\omega^2)$.

Once again the requirement that ω is upper analytic and 2π-periodic in α implies that $\sigma = -i(Ag)^{\frac{1}{2}}$ (or an integer multiple of this) and $\omega \sim \omega(0)\,e^{\xi}$ as $\xi \to -\infty$. As before, we choose $\omega(0) = -\sigma\epsilon$.

After defining $\Omega = \omega/\sigma$, (33) can be written as

$$\frac{d\Omega}{d\xi} = \frac{\Omega}{F(\Omega)}, \tag{47}$$

where

$$F(\Omega) = 1-(A+\beta)\,\Omega\frac{2+3\beta\Omega+\Omega^2+(2+\beta\Omega)[1+2\beta\Omega+\Omega^2]^{\frac{1}{2}}}{[1+2\beta\Omega+\Omega^2]^{\frac{1}{2}}(1+\beta\Omega+[1+2\beta\Omega+\Omega^2]^{\frac{1}{2}})^2}. \tag{48}$$

The solution to (47) is then uniquely determined by the condition that $\Omega \sim -\epsilon\,e^{\xi}$ for $\xi \to -\infty$.

The equations (32) which express ϕ and ψ as functions of Ω are still valid when $\beta \neq -A$. However, the square-root terms in (32) no longer produce singularities when $1+2\beta\Omega+\Omega^2 = 0$. The analyticity of these terms in a neighbourhood of $1+2\beta\Omega+\Omega^2 = 0$ can be verified by rewriting (47) as a differential equation in the function $u = [1+2\beta\Omega+\Omega^2]^{\frac{1}{2}}$. This results in an equation of the form $u_\xi = g(u)$, where $g(u)$ is analytic in a neighbourhood of $u = 0$ provided $\beta \neq -A$. The analyticity of u near $u = 0$ immediately follows. Since Ω is also analytic near $u = 0, 2\phi = 1+\Omega+u$ and $2\psi = 1-\Omega+u$ must also be analytic.

Although singularities are no longer present when $1+2\beta\Omega+\Omega^2 = 0$, other singularities can occur in $\Omega(\xi)$ when $F(\Omega) = 0$, $\Omega = \infty$, or $\Omega/F(\Omega) = 0$. We now examine each of these possibilities:

(i) $F(\Omega) = 0$: For $A \neq 1$ there are two simple roots of $F(\Omega)$ which occur

$$\Omega = \Omega_\pm = -\beta \pm i\frac{(1+A\beta)}{(1-A^2)^{\frac{1}{2}}}. \tag{49}$$

The sign of the root depends on the particular branch of $[1+2\beta\Omega+\Omega^2]^{\frac{1}{2}}$, i.e. given A and β the root $\Omega_\pm$ will correspond to one choice of branch and Ω_- to the other. A method for determining the locations $\xi_\pm$ of these roots will be given below. Since the roots are simple, it can be shown that the behaviour of $\Omega_\xi(\xi)$ near $\xi_\pm$ is given by $\Omega_\xi \sim c(\xi-\xi_\pm)^{-\frac{1}{2}}$. From (32) we see that the singular behaviour of Ω_ξ near $\xi_\pm$ leads to similar behaviour for ϕ_ξ and ψ_ξ. As a consequence the interface $z(\xi)$ possesses a curvature singularity of the form $z_{\xi\xi} \sim c_1(\xi-\xi_\pm)^{-\frac{1}{2}}$. As $\beta \to -A, \Omega_\pm \to A \pm i(1-A^2)^{\frac{1}{2}}$, which is the location of the singularities found in §4. Note also that the two roots Ω_+ and Ω_- become infinite as $A \to 1$. At $A = 1$ there are no zeros of $F(\Omega)$ for finite Ω.

(ii) $\Omega = \infty$: For Ω near ∞,

$$F(\Omega) \approx \frac{1-A}{1+\beta} + O(\Omega^{-1}) \tag{50}$$

for $A \neq 1$, and

$$F(\Omega) \approx \frac{1+\beta}{2\Omega^2} \tag{51}$$

for $A = 1$. The above limits have been calculated assuming the positive branch of the square root; choosing the negative branch leads to similar results. For $A \neq 1$ infinite values of Ω only occur at infinite values of ξ; while for $A = 1$ equation (47) is approximately

$$\frac{d\Omega}{d\xi} = \frac{2\Omega^3}{1+\beta}.$$

This equation allows singularities of the form $\Omega(\xi) \sim d(\xi-\xi_0)^{-\frac{1}{2}}$, and leads to singular behaviour in z_ξ given by $z_\xi \sim d_1(\xi-\xi_0)^{-\frac{1}{2}}$.

(iii) $\Omega/F(\Omega) = 0$: As $\Omega \to 0$, $F(\Omega)$ approaches a constant which depends on the branch of $[1+2\beta\Omega+\Omega^2]^{\frac{1}{2}}$ but which is not equal to zero. Consequently, $\Omega_\xi \sim c\Omega$ for Ω near zero and this in turn implies that $\Omega = 0$ only for finite values of ξ. Alternatively, $F(\Omega)$ can become infinite for finite values of Ω when

$$1+2\beta\Omega+\Omega^2 = 0 \tag{52}$$

or when

$$1+\beta\Omega+[1+2\beta\Omega+\Omega^2]^{\frac{1}{2}} = 0. \tag{53}$$

We have seen that the former situation does not affect the analyticity of the solution. The latter situation can only occur when the negative branch of the square root is chosen. In that case, (53) has a solution $\Omega = 0$; however, this value of Ω can only be reached for infinite values of ξ. Thus, there is no loss of analyticity which is attributable to $\Omega/F(\Omega) = 0$.

In summary, for $A \neq 1$ and $\beta \neq -A$, singularities arise only where $F(\Omega) = 0$. The singularities correspond to infinite curvature at the interface and have the same form as the curvature singularities for $\beta = -A, A \neq 1$. For $\beta \neq -A$, the asymptotic theory predicts that singularities begin away from the real (physical) axis and move towards it with constant speed σ, just as in the case, $\beta = -A$.

For $A = 1$, singularities of a different type arise due to $\Omega \to \infty$. Again the asymptotics predict that these singularities move with speed σ and eventually reach the real axis.

We can determine the location ξ of the singularities for a given value for $\Omega = \Omega(\xi)$ by integration of (47) with the requirement, $\Omega \sim -\epsilon e^{-\xi}$ as $\xi \to -\infty$. In general,

$$\begin{aligned}\xi(\Omega) &= \int_{\Omega_0}^{\Omega} \frac{F(\Omega')}{\Omega'}\,d\Omega' + \xi(\Omega_0) \\ &= \int_{\Omega_0}^{\Omega} \left(\frac{F(\Omega')}{\Omega'} - \frac{1}{\Omega'}\right) d\Omega' + \ln\Omega + (\xi(\Omega_0) - \ln\Omega_0).\end{aligned} \tag{54}$$

As $\Omega_0 \to 0$ the corresponding behaviour of $\xi(\Omega_0)$ is given by $\xi(\Omega_0) \sim \pi i + \ln\Omega_0 - \ln\epsilon$ so that (54) becomes

$$\xi(\Omega) = \int_0^{\Omega} \left(\frac{F(\Omega')}{\Omega'} - \frac{1}{\Omega'}\right) d\Omega' + \ln\Omega + \pi i - \ln\epsilon.$$

We choose $A = 1, \beta = -0.9$ as a specific case to compare the asymptotic predictions for the behaviour of the singularities with direct numerical solution of the full equations. In particular, the location ξ_s of the singularity associated with $\Omega = \infty$ is found as

$$\xi_s = \lim_{L\to\infty} \int_0^{L} \left(\frac{F(\Omega')}{\Omega'} - \frac{1}{\Omega'}\right) d\Omega' + \ln L + \pi i - \ln\epsilon.$$

Romberg integration is applied to the integral for $L = 10, 20, 40$, and we find $\xi_s + \ln\epsilon = i\pi - 0.1577$. Consequently, the trajectory of this singularity, which is an inverse square-root singularity in γ, in the complex α-plane is given by

$$\alpha = \pi + i(0.1577 + \ln\epsilon + g^{\frac{1}{2}}t). \tag{55}$$

Our code was run with 256 points and a timestep of 0.0125. The tolerance level for convergence in the interated solution of the Fredholm integral was kept at 10^{-18}; there

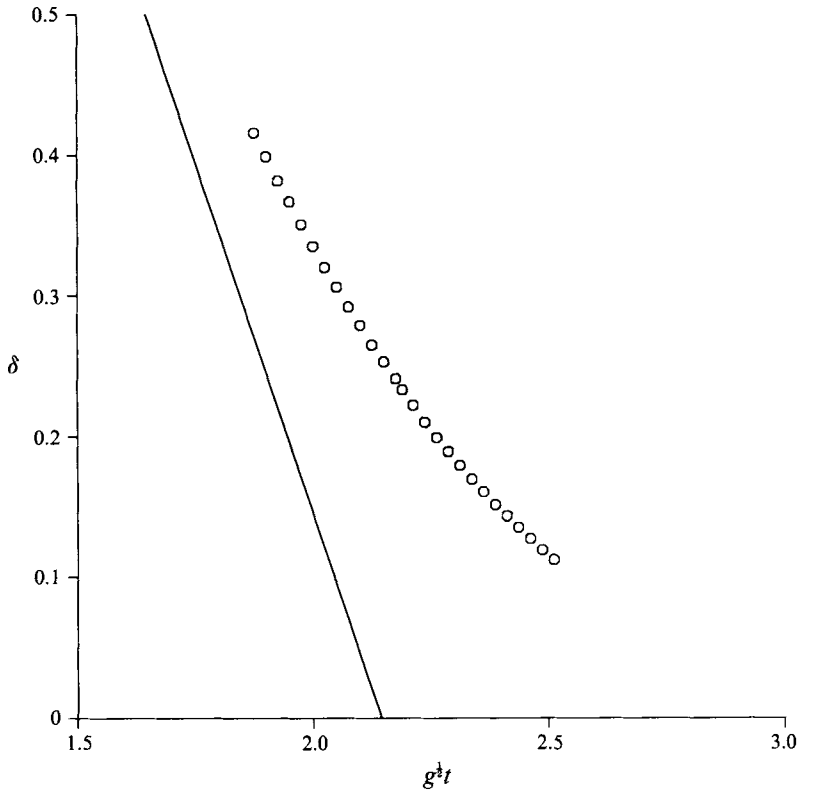

FIGURE 8. The distance of the singularity from the real axis when $A = 1$, $\beta = -0.9$. The solid line shows the asymptotic prediction; the circles give the numerical values.

was no need to filter. Since the singularity moves along $\alpha_r = \pi$, the form fit is much easier to implement. In figure 8, we show the distance δ of the singularity away from the real axis. Also shown is the predicted trajectory. Clearly the singularity is slowing down dramatically as it approaches the real axis. It is quite plausible that the singularity never reaches the real axis in finite time.

7. Conclusions

The asymptotic theory predicts the existence of singularities in the complex plane of the Lagrangian variables. A special family of solutions contains singularities that move steadily towards the real axis and reach it in finite time. When $\beta = -A$, this family may be expressed in simple terms. Numerical calculations of the full equations confirm this behaviour for $A \leqslant 0.9$. However, as $A \to 1$, the singularities slow down as they get close to the real axis. Additional nonlinear effects, neglected by the asymptotic theory, come into play. Also, the profiles are quite deformed by the time the singularities get close to the real axis.

For $A = 1$, the special travelling wave solution contains a zero in z_α instead of singularities through a loss in analyticity. A zero in z_α indicates a failure in the conformal map between α and z. When the zero reaches the real axis, a geometric singularity in the interface will occur. Although such a singularity would not be revealed in the Fourier spectra or affect the ability of the computations to proceed, it would cause a blow up in curvature (cusp) on the interface. Our calculations show that

this does not occur. Instead the zero moves towards, but does not reach, the real axis in finite time.

When $\beta \neq -A$ and $A = 1$, a travelling wave solution can be found that contains a singularity. This singularity moves downwards to $\alpha_r = \pi$ until it reaches the real axis in finite time. Once again, numerical calculations show a slow down in the motion of the singularity when it gets close to the real axis.

When A is near or equal to 1, our numerical calculations do not indicate whether the singularities reach the real axis in finite time. Nevertheless, we are led to the following speculation. For $A < 1$, the singularity does reach the real axis in finite time, but the closer A is to 1, the longer the time. When $A = 1$, the singularity does not reach the real axis in finite time.

This work was supported in part by the Air Force Office of Scientific Research through grant number AFOSR-90-0003; the National Science Foundation through grant numbers NSF DMS90-0588 and NSF DMS90-05932; and a National Science Foundation Postdoctoral Research Fellowship. Most of our computing was done at the Ohio Supercomputer Center, and we gratefully acknowledge the support and computer resources we received.

Appendix A

We present a brief derivation of the system of localized approximation equations appearing in (24). Let $z(\alpha, t) = \alpha + s(\alpha, t)$ and write the analytically extended equations (15) in the form

$$\frac{\partial s^*}{\partial t}(\alpha, t) = I[s, \gamma](\alpha, t) + \frac{\beta\gamma(\alpha, t)}{2z_\alpha(\alpha, t)}, \tag{A 1}$$

$$\frac{\partial \gamma}{\partial t}(\alpha, t) = G[q, q^*, s, s^*, \gamma](\alpha, t), \tag{A 2}$$

where

$$I[s, \gamma](\alpha, t) = q^* = \frac{1}{2\pi i}\,\mathrm{PV}\int_{-\infty}^{\infty} \frac{\gamma(\alpha+\zeta)}{z(\alpha, t) - z(\alpha+\zeta, t)}\,d\zeta, \tag{A 3}$$

$$G[q, q^*, s, s^*, \gamma](\alpha, t) = A\left[q_t^* z_\alpha + q_t z_\alpha^* - \frac{\beta\gamma}{2}\left(\frac{q_\alpha}{z_\alpha} + \frac{q_\alpha^*}{z_\alpha^*}\right) - ig(z_\alpha - z_\alpha^*)\right] + \frac{A+2\beta}{4}\frac{\partial}{\partial\alpha}\left(\frac{\gamma^2}{z_\alpha z_\alpha^*}\right). \tag{A 4}$$

Assume that s and γ are analytic in the strip $|\mathrm{Im}\{\alpha\}| < \rho$ and decompose as in (17), (18) so that

$$s(\alpha, t) = s_+(\alpha, t) + s_-(\alpha, t), \quad \gamma(\alpha, t) = \gamma_+(\alpha, t) + \gamma_-(\alpha, t), \tag{A 5}$$

with s_+, s_-, γ_+ and γ_- defined in (18).

We first show how the approximation is applied to (A 1). Write the term $I[s, \gamma]$ as

$$I[s, \gamma] = I[s_+, \gamma_+] + I[s_-, \gamma_-] + E[s_+, s_-, \gamma_+, \gamma_-], \tag{A 6}$$

with

$$I[s_+, \gamma_+] = \frac{1}{2\pi i}\,\mathrm{PV}\int_{-\infty}^{\infty} \frac{\gamma_+(\alpha+\zeta, t)}{-\zeta + s_+(\alpha, t) - s_+(\alpha+\zeta, t)}\,d\zeta, \tag{A 7}$$

and a similar expression for $I[s_-, \gamma_-]$. Equation (A 6) may be regarded as the definition

of the error term E. The assumptions in our approximation imply that the term E is negligible. Thus,

$$I[s,\gamma] \sim I[s_+,\gamma_+]+I[s_-,\gamma_-]. \tag{A 8}$$

We assume that $|s_{\alpha+}(\alpha)| < 1$ for $\mathrm{Im}\{\alpha\} \geqslant 0$. Consequently, $|s_+(\alpha)-s_+(\alpha+\zeta)| < |\zeta|$ for $\mathrm{Im}\{\alpha\} \geqslant 0$, so that in the upper half-plane of α the only singularity of the integrand in q^* is at $\zeta = 0$. Thus we can equate the principal value integral (A 7) to the sum of two contour integrals as

$$\begin{aligned} I[s_+,\gamma_+] = &-\frac{1}{2\pi\mathrm{i}}\lim_{R\to\infty}\mathrm{PV}\int_{\substack{|\zeta|=R\\ \mathrm{Im}\{\zeta\}>0}}\frac{\gamma_+(\alpha+\zeta,t)}{-\zeta+s_+(\alpha,t)-s_+(\alpha+\zeta,t)}\mathrm{d}\zeta \\ &+\frac{1}{2\pi\mathrm{i}}\lim_{\delta\to 0}\mathrm{PV}\int_{\substack{|\zeta|=\delta\\ \mathrm{Im}\{\zeta\}>0}}\frac{\gamma_+(\alpha+\zeta,t)}{-\zeta+s_+(\alpha,t)-s_+(\alpha+\zeta,t)}\mathrm{d}\zeta. \end{aligned} \tag{A 9}$$

The first integral vanishes as $R\to\infty$ (see Siegel 1989 for details). The second integral can be evaluated by using the residue theorem:

$$I[s_+,\gamma_+] = q^*_-(\alpha,t) = -\frac{1}{2}\frac{\gamma_+(\alpha)}{1+s_{\alpha+}(\alpha)}. \tag{A 10}$$

The factor of $\frac{1}{2}$ comes from integration over a half-circle.

Similarly, if $|s_{\alpha-}(\alpha)| < 1$ for $\mathrm{Im}\{\alpha\} \leqslant 0$ then $I[s_-,\gamma_-]$ can be evaluated by integration over a contour in the lower half-plane, yielding

$$I[s_-,\gamma_-] = q^*_+(\alpha) = \frac{1}{2}\frac{\gamma_-(\alpha)}{1+s_{\alpha-}(\alpha)}. \tag{A 11}$$

Under the assumptions of our approximation, the other term in (A 1) may be decomposed as

$$\frac{\gamma(\alpha)}{z_\alpha(\alpha)} = \frac{\gamma_+(\alpha)}{1+s_{\alpha+}(\alpha)}+\frac{\gamma_-(\alpha)}{1+s_{\alpha-}(\alpha)}. \tag{A 12}$$

By combining the results (A 10), (A 11), (A 12), we find that (A 1) can be approximated by

$$\frac{\partial}{\partial t}(s^*_+(\alpha)+s^*_-(\alpha)) = \frac{\beta-1}{2}\frac{\gamma_+}{1+s_{\alpha+}}+\frac{\beta+1}{2}\frac{\gamma_-}{1+s_{\alpha-}}. \tag{A 13}$$

The projection of this equation onto the space of functions analytic in the upper half-plane leads directly to (24*a*), namely

$$\frac{\partial s^*}{\partial t} = \frac{\beta-1}{2}\frac{\gamma_+}{1+s_{\alpha+}}. \tag{A 14}$$

The other equation may be obtained by projecting onto the space of functions analytic in the lower half plane, and by applying the $*$-operator. Recall that the $*$-operator switches $+$ components to $-$ components (20), and that $\gamma^*_+ = \gamma_-$ (21). Thus,

$$\frac{\partial s_+}{\partial t} = \frac{\beta+1}{2}\frac{\gamma_+}{1+s^*_{\alpha-}}. \tag{A 15}$$

The approximation to (A 2) is derived in a similar fashion. First, we write

$$G[q,q^*,s,s^*,\gamma] = G_+[q_+,q^*_-,s_+,s^*_-,\gamma_+]+G_-[q_-,q^*_+,s_-,s^*_+,\gamma_-],$$

where

$$G_+[q_+, q_-^*, s_+, s_-^*, \gamma_+] = A\left[q_{t-}^*(1+s_{\alpha+}) + q_{t+}(1+s_{\alpha-}^*) - \frac{\beta\gamma_+}{2}\left(\frac{q_{\alpha+}}{1+s_{\alpha+}} + \frac{q_{\alpha-}^*}{1+s_{\alpha-}^*}\right) - \mathrm{i}g(s_{\alpha+} - s_{\alpha-}^*)\right] + \frac{A+2\beta}{4}\frac{\partial}{\partial\alpha}\left(\frac{\gamma_+^2}{(1+s_{\alpha+})(1+s_{\alpha-}^*)}\right). \quad \text{(A 16)}$$

$G_-[q_-, q_+^*, s_-, s_+^*, \gamma_-]$ is defined similarly.

We may differentiate (A 10), (A 11) with respect to t;

$$q_{t+} = \frac{1}{2}\left[\frac{\gamma_{t+}}{1+s_{\alpha-}^*} - \frac{\gamma_+ s_{\alpha t-}^*}{(1+s_{\alpha-}^*)^2}\right], \quad q_{t-}^* = -\frac{1}{2}\left[\frac{\gamma_{t+}}{1+s_{\alpha+}} - \frac{\gamma_+ s_{\alpha t+}}{(1+s_{\alpha+})^2}\right]. \quad \text{(A 17)}$$

In addition, we differentiate (A 14), (A 15) with respect to α, and the results, combined with (A 17), may be used to obtain the intermediate result

$$q_{t-}^*(1+s_{\alpha+}) + q_{t+}(1+s_{\alpha-}^*) = \frac{\beta-1}{4}\frac{\gamma_+^2 s_{\alpha\alpha+}}{(1+s_{\alpha+})^2(1+s_{\alpha-}^*)} - \frac{\beta+1}{4}\frac{\gamma_+^2 s_{\alpha\alpha-}^*}{(1+s_{\alpha+})(1+s_{\alpha-}^*)^2} + \frac{1}{2}\frac{\gamma_{\alpha+}\gamma_+}{(1+s_{\alpha+})(1+s_{\alpha-}^*)}. \quad \text{(A 18)}$$

In the same way, we find

$$\frac{q_{\alpha+}}{1+s_{\alpha+}} + \frac{q_{\alpha-}^*}{1+s_{\alpha-}^*} = \frac{\gamma_+}{2}\left[\frac{s_{\alpha\alpha+}}{(1+s_{\alpha+})^2(1+s_{\alpha-}^*)} - \frac{s_{\alpha\alpha-}^*}{(1+s_{\alpha+})(1+s_{\alpha-}^*)^2}\right]. \quad \text{(A 19)}$$

Finally, by substituting (A 18), (A 19) into (A 16), and simplying, we obtain

$$G_+[q_+, q_-^*, s_+, s_-^*, \gamma_+] = \frac{A+\beta}{2}\frac{\partial}{\partial\alpha}\left(\frac{\gamma_+^2}{(1+s_{\alpha+})(1+s_{\alpha-}^*)}\right) - \mathrm{i}Ag(s_{\alpha+} - s_{\alpha-}^*). \quad \text{(A 20)}$$

Equation (24c) follows by projecting this result onto the space of functions analytic in the upper half-plane. Since $\gamma_- = \gamma_+^*$, an equation for $\partial\gamma_-/\partial t$ is unnecessary.

Appendix B

First we describe the numerical construction of the initial profiles (35) to the travelling wave solutions (32), (34). By expanding the square root with the help of the software package MATHEMATICA, we obtain

$$[1+2A\eta+\eta^2]^{\frac{1}{2}} = 1 + \sum_{k=1} a_k \eta^k, \quad \text{(B 1)}$$

where the first few values of the coefficients are

$$\left.\begin{aligned} a_1 &= A, \quad a_2 = \frac{1-A^2}{2}, \quad a_3 = -\frac{A(1-A^2)}{2}, \\ a_4 &= -\frac{(1-A^2)(1-5A^2)}{8}, \quad a_5 = \frac{A(1-A^2)(3-7A^2)}{8}. \end{aligned}\right\} \quad \text{(B 2)}$$

Since $\eta = \epsilon\exp(\mathrm{i}\alpha)$ determines the initial profiles, we obtain

$$\left.\begin{aligned} x(\alpha) &= \alpha + \sum_{k=1}\frac{\epsilon^k a_k}{k}\sin(k\alpha), \quad y(\alpha) = H + \epsilon\cos(\alpha) \\ \gamma(\alpha) &\equiv \mu_\alpha(\alpha) = -2\epsilon(Ag)^{\frac{1}{2}}\sin(\alpha). \end{aligned}\right\} \quad \text{(B 3)}$$

From (36), we find $H = -0.5\epsilon^2 A$.

Unfortunately, close to 30 terms are necessary to specify the initial profile with the accuracy available in double precision on a CRAY YMP computer. Consequently, we determined the initial conditions by spectral techniques. The Fourier coefficients for $x_\alpha, y_\alpha, \mu_\alpha$ may be determined directly by use of the fast Fourier transform. Their integrals may then be performed analytically, and evenly spaced points along the interface determined through the inverse fast Fourier transform. Typically, the number of points used in the discrete transforms was the same number used in the calculations of the evolution of the interface. Since a filter level no lower than 10^{-18} was used in the evolution of the interface, only about 18 terms are truly necessary. In fact we observed no significant changes in the results if only two terms were used. In conclusion, the initial condition was determined sufficiently accurately for the purposes of our study.

The series representation (B 3) did prove useful in determining the profile predicted by linear analysis of (7), (8) and shown in figure 1;

$$x = \alpha + A\epsilon \exp\{(Ag)^{\frac{1}{2}} t\} \sin(\alpha) + \sum_{k=2} \frac{\epsilon^k a_k}{k} \sin(k\alpha),$$

$$y = -\tfrac{1}{2}\epsilon^2 A + \epsilon \exp\{(Ag)^{\frac{1}{2}} t\} \cos(\alpha).$$

Only a few terms in the sum are needed for plotting accuracy.

To obtain the profiles for the predictions of standard linear theory in the Eulerian frame, we first determine the values of α that give evenly spaced values for x. Then we evaluate y, γ at these values of x, and by using the discrete Fourier transform, we obtain their Fourier coefficients. According to the linear theory, if $y = C\cos(kx), \gamma = 2(Agk)^{\frac{1}{2}} D \sin(kx)$ initially, then

$$y = 0.5(C-D)\exp\{(Agk)^{\frac{1}{2}} t\}\cos(kx) + 0.5(C+D)\exp\{-(Agk)^{\frac{1}{2}} t\}\cos(kx).$$

Consequently, the amplitude of each mode can be determined and the profile constituted by an inverse discrete Fourier transform. Plotting accuracy is obtained for $t = 2.0(Ag)^{-\frac{1}{2}}$ with 16 modes.

To obtain the profiles for the predictions of the asymptotic theory in this paper, ϵ is simply replaced by $\epsilon \exp\{(Ag)^{\frac{1}{2}} t\}$ in (55). It can be shown that the asymptotic equations (26) preserve the mean height of the interface. Consequently, $H = -0.5\epsilon^2 \exp\{2(Ag)^{\frac{1}{2}} t\}$ in (55).

REFERENCES

BAKER, G. R. 1983 Generalized vortex methods for free-surface flows. In *Waves on Fluid Interfaces* (ed. R. E. Meyer). Academic.

BAKER, G. R. 1990 Singularities in the complex physical plane. In *Hyperbolic Problems* (ed. B. Engquist & B. Gustafsson). Lund: Studentlitteratur.

BAKER, G. R., MCCRORY, C. P., VERDON, C. P. & ORSZAG, S. A. 1987 Rayleigh–Taylor instability of fluid layers. *J. Fluid Mech.* **178**, 161–175.

BAKER, G. R., MEIRON, D. I. & ORSZAG, S. A. 1980 Vortex simulations of the Rayleigh–Taylor instability. *Phys. Fluids* **23**, 1485–1490.

BAKER, G. R., MEIRON, D. I. & ORSZAG, S. A. 1982 Generalized vortex methods for free-surface flow problems. *J. Fluid Mech.* **123**, 477–501.

BAKER, G. R., MEIRON, D. I. & ORSZAG, S. A. 1984 Boundary integral methods for axisymmetric and three-dimensional Rayleigh–Taylor instability problems. *Physica D* **12**, 19–31.

BAKER, G. R. & MOORE, D. W. 1989 The rise and distortion of a two-dimensional gas bubble in an inviscid liquid. *Phys. Fluids* A **1**, 1451–1459.

BAKER, G. R. & SHELLEY, M. J. 1990 On the connection between thin vortex layers and vortex sheets. *J. Fluid Mech.* **215**, 161–194.

BIRKHOFF, G. 1962 Helmholtz and Taylor instabilities. In *Proc. Sympos. Appl. Maths*, vol. XII. Providence, R.I.: AMS.

CAFLISCH, R. & ORELLANA, O. 1986 Long time existence for a slightly perturbed vortex sheet. *Commun. Pure Appl. Maths* **39**, 807–816.

CAFLISCH, R., ORELLANA, O. & SIEGEL, M. 1990 A localized approximation method for vortical flows. *SIAM J. Appl. Maths* **50**, 1517–1532.

COWLEY, S. J., BAKER, G. R., TANVEER, S. & PAGE, M. 1993 An asymptotic description of the formation of a Moore singularity in a vortex sheet. *J. Fluid Mech.* (submitted).

DELORT, J. 1991 Existence de nappes de tourbillon en dimension deux. *C.R. Acad. Sci. Paris* I *Maths* **312**, 85–88.

DIPERNA, R. & MAJDA, A. 1987 Concentrations in regularizations for 2-d incompressible flow. *Commun. Pure Appl. Maths* **60**, 301–345.

DUCHON, J. & ROBERT, O. 1988 Global vortex sheet solutions of euler equations in the plane. *J. Diff Equat.* **73**, 215–224.

ELY, J. & BAKER, G. R. 1993 High-precision calculations of vortex sheet motion. *J. Comput. Phys.* (submitted.)

KELVIN, LORD 1871 Hydro-kinetic solutions and observations. *Phil. Mag.* **42**(4), 362–377.

KERR, R. M. 1986 Analysis of Rayleigh–Taylor flows using vortex blobs. *Rep.* UCID-20915. Lawrence Livermore National Laboratory.

KRASNY, R. 1986*a* Desingularization of periodic vortex sheet roll-up. *J. Comput. Phys.* **65**, 292–313.

KRASNY, R. 1986*b* On singularity formation in a vortex sheet and the point vortex approximation. *J. Fluid Mech.* **167**, 65–93.

MEIRON, D. I., BAKER, G. R. & ORSZAG, S. A. 1982 Analytic structure of vortex sheet dynamics. Part 1. Kelvin–Helmholtz instability. *J. Fluid Mech.* **114**, 283–298.

MOORE, D. W. 1979 The spontaneous appearance of a singularity in the shape of an evolving vortex sheet. *Proc. R. Soc. Lond.* A **365**, 105–119.

MOORE, D. W. 1982 A vortex method applied to interfacial waves. In *Vortex Motion* (ed. H. G. Hornung & E. A. Muller). Vieweg & Sons.

MOORE, D. W. 1985 Numerical and analytical aspects of Helmholtz instability. In *Theoretical and Applied Mechanics* (ed. F. I. Niordson & N. Olhoff). Elsevier.

PUGH, D. A. 1989 Development of vortex sheets in Boussinesq flows – formation of singularities. PhD thesis, Imperial College.

PUGH, D. & COWLEY, S. 1993 On the formation of an interface singularity in the rising two-dimensional Boussinesq bubble. *J. Fluid Mech.* (to appear).

SAFFMAN, P. G. & BAKER, G. R. 1979 Vortex interactions. *Ann. Rev. Fluid Mech.* **11**, 95–122.

SHARP, D. H. 1984 An overview of Rayleigh–Taylor instability. *Physica D* **12**, 3–18.

SHELLEY, M. J. 1992 A study of singularity formation in vortex sheet motion by a spectrally accurate method. *J. Fluid Mech.* **244**, 493–526.

SOEGEL, M. 1989 An analytical and numerical study of singularity formation in the Rayleigh–Taylor problem. PhD thesis, New York University.

TANVEER, S. 1992 Singularities in the classical Rayleigh–Taylor flow: formation and subsequent motion. *Proc. R. Soc. Lond.* A (submitted).

TRYGGVASON, G. 1988 Numerical simulations of the Rayleigh–Taylor instability. *J. Comput. Phys.* **75**, 253–282.